

2000

Studies in hard pion photoproduction

Christian Jens Wahlquist
College of William & Mary - Arts & Sciences

Follow this and additional works at: <https://scholarworks.wm.edu/etd>



Part of the [Physics Commons](#)

Recommended Citation

Wahlquist, Christian Jens, "Studies in hard pion photoproduction" (2000). *Dissertations, Theses, and Masters Projects*. Paper 1539623996.

<https://dx.doi.org/doi:10.21220/s2-9r18-p246>

This Dissertation is brought to you for free and open access by the Theses, Dissertations, & Master Projects at W&M ScholarWorks. It has been accepted for inclusion in Dissertations, Theses, and Masters Projects by an authorized administrator of W&M ScholarWorks. For more information, please contact scholarworks@wm.edu.

INFORMATION TO USERS

This manuscript has been reproduced from the microfilm master. UMI films the text directly from the original or copy submitted. Thus, some thesis and dissertation copies are in typewriter face, while others may be from any type of computer printer.

The quality of this reproduction is dependent upon the quality of the copy submitted. Broken or indistinct print, colored or poor quality illustrations and photographs, print bleedthrough, substandard margins, and improper alignment can adversely affect reproduction.

In the unlikely event that the author did not send UMI a complete manuscript and there are missing pages, these will be noted. Also, if unauthorized copyright material had to be removed, a note will indicate the deletion.

Oversize materials (e.g., maps, drawings, charts) are reproduced by sectioning the original, beginning at the upper left-hand corner and continuing from left to right in equal sections with small overlaps.

Photographs included in the original manuscript have been reproduced xerographically in this copy. Higher quality 6" x 9" black and white photographic prints are available for any photographs or illustrations appearing in this copy for an additional charge. Contact UMI directly to order.

**Bell & Howell Information and Learning
300 North Zeeb Road, Ann Arbor, MI 48106-1346 USA
800-521-0600**

UMI[®]

STUDIES IN HARD PION PHOTOPRODUCTION

A Dissertation

Presented to The Faculty of the Department of Physics

The College of William and Mary

In Partial Fulfillment

Of the Requirements for the Degree of

Doctor of Philosophy

By

Christian Jens Wahlquist

August 2000

UMI Number: 9999059

**Copyright 2000 by
Wahlquist, Christian Jens**

All rights reserved.

UMI[®]

UMI Microform 9999059

Copyright 2001 by Bell & Howell Information and Learning Company.

**All rights reserved. This microform edition is protected against
unauthorized copying under Title 17, United States Code.**

**Bell & Howell Information and Learning Company
300 North Zeeb Road
P.O. Box 1346
Ann Arbor, MI 48106-1346**

APPROVAL SHEET


This dissertation is submitted in partial fulfillment
of the requirements for the degree of

Doctor of Philosophy.



Christian Jens Wahlquist

Approved, August 2000



Carl E. Carlson



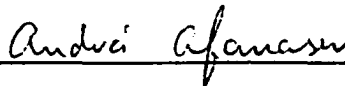
Christopher Carone



Keith Griffioen



Marc Sher



Andrei Afanasev

North Carolina Central University

Copyright
by
Christian Jens Wahlquist
2000

Contents

Acknowledgments	vii
List of Figures	viii
Abstract	x
Chapter 1 INTRODUCTION	2
1.1 History of Bjorken Scaling and Partons	2
1.2 Interpretation of F_1 and F_2 Using Parton Distributions	5
1.3 Polarized Structure Functions	7
1.4 Outline of the Thesis	8
Chapter 2 Probing polarized parton distributions with meson photoproduction	10
2.1 Motivation	10
2.2 Calculations	13
2.3 Results	17
2.4 Discussion	21
Chapter 3 Measuring polarized gluon and quark distributions with meson photoproduction	24
3.1 Motivation	24
3.2 Calculations	27
3.3 Results without Polarization	33
3.4 Results with Polarization	38
3.5 Discussion	45
Chapter 4 Soft Contributions to Hard Pion Photoproduction	51
4.1 Introduction	51
4.2 Outline of Calculations	53

4.3	Some Results	57
4.4	Discussion	60
Chapter 5 Scaling and Duality in Semi-exclusive Processes		65
5.1	Introduction	65
5.2	kinematic variables	67
5.3	scaling and kinematic regions	70
5.4	resonance bumps vs. the scaling curve	76
5.5	Conclusions and Discussion	77
Appendix A fragmentation functions		81
A.1	Carlson-Wakely fragmentation functions	81
A.2	Newer form of Carlson-Wakely	82
Bibliography		83
Vita		88

Acknowledgments

I would like to thank my advisor, Dr. Carl Carlson for his guidance throughout my stay at William and Mary. I would also like to thank Dr. Andrei Afanasev for his invaluable input into our collaboration. Last I would like to thank my wife Dari Wahlquist for all of her support through my graduate studies.

List of Figures

1.1	a) elastic scattering off of the proton b) deep inelastic scattering off of the proton.	3
1.2	The quark parton model of deep inelastic scattering	4
2.1	One lowest order perturbative diagram for direct photoproduction of mesons from a quark. There are four diagrams total, corresponding to the four places a photon may be attached to a quark line.	11
2.2	Comparing direct and fragmentation photoproduction of π^+ off protons, for $E_\gamma = 30$ GeV and $\theta_{lab} = 5^\circ$. The solid line is direct production of π^+ and the dotted line is fragmentation production of π^+ . For reference, the dashed line shows direct production of π^0 . The abscissa is $k = \vec{k} $ in the lab.	16
2.3	The upper three curves are the helicity dependent asymmetries for π^+ photoproduction off the proton, for 30 GeV photons and lab angle 5 or 14° . The solid line is for the GRSV polarized quark distributions; the dashed line is for GS; and the dotted line is for the suggestion of Soffer <i>et al.</i> GRSV is about the same as GS for the π^+ case. The lower three curves are for π^- photoproduction. GRSV and GS are well separated in the π^- case.	19
2.4	Polarization asymmetry results for 50 GeV incoming electrons, with pions emerging at 5° lab angle and the electrons not observed. We have integrated over the energies and polarizations of the virtual (but on the average low Q^2) photons with weightings as indicated in the text. The upper three curves are for the π^+ and the lower three curves are for the π^- . The solid, dashed, and dotted lines are for GRSV, GS, and Soffer <i>et al.</i> , respectively.	20
3.1	A number of polarized gluon distributions, all normalized to the unpolarized BBS gluon distribution. The sources of these distributions are given later in the text.	26
3.2	One diagram for photoproducing π mesons via fragmentation.	28
3.3	A resolved photon process.	31

3.4	Comparing fragmentation, direct, and resolved photon processes for $e + p \rightarrow \pi^+ + X$ with $E_e = 50$ GeV and $\theta_{lab} = 5.5^\circ$. These all use the GRSV parton distributions. The relative size of the contributions should not depend much on which parton distributions used. For the resolved photon contribution [33], the result of both the perturbative splitting function for the photon, and the more sophisticated SaS 2D are shown. Both are small for these kinematics.	34
3.5	The π^+/π^- ratio for $E_e = 50$ GeV and $\theta_{lab} = 5.5^\circ$ for the pions. The dashed curve is for GRV and the solid curve is for CTEQ. Both have $u(x)/d(x) \sim 1/(1-x)$ for large x . The four pairs of curves are for, top to bottom, protons, a target which is 5/9 protons and 4/9 neutrons, an isoscalar target, and neutrons.	35
3.6	Detail of π^+/π^- ratio for $E_e = 50$ GeV and $\theta_{lab} = 5.5^\circ$ for the pions, for a target which is 5/9 protons and 4/9 neutrons.	37
3.7	The asymmetry E for $\vec{\gamma} + \vec{n} \rightarrow \pi^\pm + X$, at $E_e = 50$ GeV and $\theta_{lab} = 5.5^\circ$. The upper six curves are for π^- production and the lower six curves are for π^+ production. For each set of six, there are three curves with the full calculation, with the loose dotted curve using parton distributions from GRSV, the dashed curve using GS-A, and the tight dotted line using CTEQ/Soffer <i>et al.</i> and the BBS polarized gluon distribution. The other three curves have Δg set to zero, with the solid line using GRSV, the dash-dot curve using GS, and the dash-triple dot curve using CTEQ/Soffer <i>et al.</i>	39
3.8	The asymmetry E for $\vec{\gamma} + \vec{p} \rightarrow \pi^\pm + X$, at $E_e = 50$ GeV and $\theta_{lab} = 5.5^\circ$. This time, the upper six curves are for π^+ production and the lower six curves are for π^- production. As in Fig. 3.4, for each set of six, there are three curves with the full calculation, with the loose dotted curve using parton distributions from GRSV, the dashed curve using GS-A, and the tight dotted line using CTEQ/Soffer <i>et al.</i> and the BBS polarized gluon distribution. The other three curves have Δg set to zero, with the solid curve using GRSV, the dash-dot curve using GS, and the dash-triple dot curve using CTEQ/Soffer <i>et al.</i>	40
3.9	The asymmetry E for $\vec{\gamma} + \vec{n} \rightarrow \pi^\pm + X$, at $E_e = 50$ GeV and $\theta_{lab} = 5.5^\circ$, with one model for the quark distributions and several models for the polarized gluon distribution. I choose to use the quark distributions of GS. The solid curve is the benchmark with Δg set to zero. The short dashed curve uses the quark and unpolarized gluon distribution of GS but the polarized gluon distribution of GS model A. The long dashed curve uses GS model C. The dash dot curve uses GRSV. The dash triple dot curve similarly uses BBS, the tight dotted curve uses BFR model AR, and the loose dotted curve uses BFR model OS.	43

3.10	The asymmetry E for $\bar{\gamma} + \bar{n} \rightarrow \pi^{\pm} + X$, at $E_e = 27.5$ GeV and $\theta_{lab} = 5.5^{\circ}$. The remainder of the caption is the same as for Fig. 3.4.	44
3.11	The asymmetry E for $\bar{\gamma} + \bar{p} \rightarrow \pi^{\pm} + X$, at $E_e = 27.5$ GeV and $\theta_{lab} = 5.5^{\circ}$. The remainder of the caption is the same as for Fig. 3.4.	46
3.12	The asymmetry E for $\bar{\gamma} + \bar{p} \rightarrow \pi^{\pm} + X$, at $E_e = 27$ GeV and $\theta_{lab} = 5.5^{\circ}$, with one model for the quark distributions and several models for the polarized gluon distribution. I use the quark distributions of GS. The upper set of curves is for the π^+ and the lower set is for the π^- ; otherwise the caption is the same as Fig 3.4.	48
4.1	The invariant differential cross sections for $ep \rightarrow \pi^- X$, above, and π^+ , below. The incoming electron energy is 50 GeV, and pion lab angle is 5.5°	58
4.2	The calculated pion to electron ratio for a ^{15}N He_3 target. For this target and this vertical scale, the π^- results are hardly distinct from the π^+ . They are in reasonable accord with data as reported in [32].	59
4.3	Polarization asymmetries for $ep \rightarrow \pi^-$, above and π^+ , below. The data for charged hadrons and for charged pions is from [32].	61
4.4	Polarization asymmetries for the deuteron, with $ed \rightarrow \pi^- X$ above and $ed \rightarrow$ $\pi^+ X$ below. The data is from [32].	62
4.5	The differential cross section for 340 GeV electrons impinging on an standing proton with positive pions emerging at 1.34° . (This corresponds to a collider with 4 GeV electrons hitting 40 GeV protons and pions emerging at 90° in the lab.)	64
5.1	Direct (also isolated or short-distance) pion production, with some kinematics indicated.	68
5.2	Soft processes, approximated by vector meson dominance.	71
5.3	A fragmentation process, with the pion's momentum labeled as k	71
5.4	Kinematic regions relevant to studying duality in $\gamma N \rightarrow \pi X$ for 30 GeV incoming photons. The upper dashed-dotted line is the overall kinematic limit, and corresponds to $\gamma N \rightarrow \pi N$. The other solid and dotted elliptical lines have m_X of 2 and 3.5 GeV, respectively. Between the solid and dashed- dotted elliptical lines lies the resonance region. Above the grey line soft processes and fragmentation processes are small, and direct pion production dominates. Hence the region between the grey line and the solid elliptical line is the region that can be smoothly compared to the resonance region. The dashed elliptical curve is for x fixed at 0.7.	80

Abstract

The production of high transverse momenta mesons via polarized photoproduction can be a means of determining the parton structure of the target. At the regions of highest transverse pion momenta, k_T , it can be shown that short distance, direct, pion production dominates and is sensitive to the polarized quark distributions. As the produced pions transverse momenta decreases the importance of pions produced through fragmentation following photon-gluon fusion increases. This process give us sensitivity to the form of the polarized gluon distribution. Both processes are calculable with perturbative Quantum Chromodynamics (pQCD) due to the high k_T of the pion produced. Numerical results are presented for conditions in current g_1 experiments. In order to determine the region in which the k_T is sufficient for the use of pQCD, and to separate the desired processes from unwanted background functions, a calculation of the soft processes is undertaken. Vector meson dominance is the largest contributor to the soft processes and can be large enough to make a measurement of the asymmetries susceptible to the polarized gluon distributions difficult at the kinematics of existing g_1 experiments. Once all of the contributions are known I can use the above processes to extend Bloom-Gilman scaling and duality to semi-exclusive processes. It will be shown that the scaling behavior should exist for the direct process and that regions where this process is dominant do exist. I will also show that the constancy with changing momentum transfer of the resonance peak/scaling curve ratio, familiar for many resonances in deep inelastic scattering, is also expected in the semi-exclusive case.

STUDIES IN HARD PION PHOTOPRODUCTION

Chapter 1

INTRODUCTION

1.1 History of Bjorken Scaling and Partons

In the late 1960's there were a series of experiments at the Stanford Linear Accelerator (SLAC) that established that nucleons were composed of point particles called partons. Measurements of the form factors of the proton using elastic scattering, Fig. 1.1 had established that the proton was not a point-like particle but had a radius of ≈ 1 fm.

At higher energies one frequently stops scattering elastically off of the proton and starts smashing the proton into pieces. However, by increasing the energy of the exchanged photon its wavelength can be shortened enough to start to resolve the substructure of the proton. An example of this deep inelastic scattering (DIS) can be seen in Fig. 1.1.

Functions other than the form factors from elastic scattering are needed to describe the new dynamics. Splitting the interaction into two parts, one has the leptonic tensor, $L_{\mu\nu}^e$, unchanged from elastic scattering and the hadronic tensor, $W^{\mu\nu}$. While the leptonic tensor was known, there was no established theory to determine the structure of the proton.

The interaction was known to have properties such as gauge invariance and was

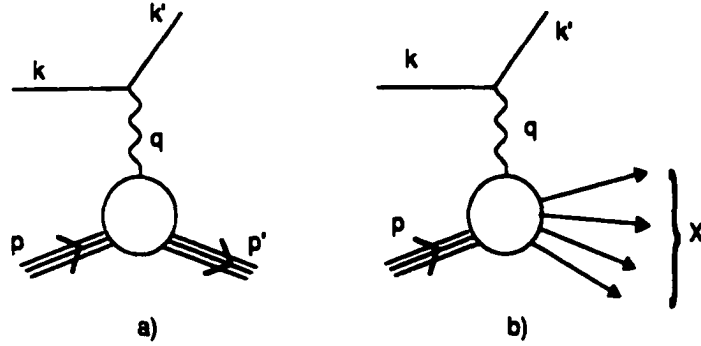


Figure 1.1: a) elastic scattering off of the proton b) deep inelastic scattering off of the proton.

also known to obey certain discrete symmetries. The hadronic tensor in the unpolarized case should only depend on the incoming four momenta p and q , the momentum of the incoming proton and virtual photon respectively. Using these properties the unpolarized hadronic tensor may be written in the most general way possible as

$$W^{\mu\nu} = W_1 \left(-g^{\mu\nu} + \frac{q^\mu q^\nu}{q^2} \right) + W_2 \frac{1}{M_p^2} \left(p^\mu - \frac{p \cdot q}{q^2} q^\mu \right) \left(p^\nu - \frac{p \cdot q}{q^2} q^\nu \right) \quad (1.1)$$

with M_p being the mass of the proton. All of the reactions due to the structure of the proton is folded into the two functions W_1 and W_2 .

Using the impulse approximation, assuming that the interaction of the photon with the partons is short in duration when compared to the timescale of the partons interaction with each other, one could describe DIS as scattering off of one of the constituent partons in the nucleon. If the photon scatters off of a point-like particle within the proton, it can be shown that the structure functions are dependent on only one variable, x_{bj} , where

$$x_{bj} = Q^2/2q \cdot p \text{ and } Q^2 = -q^2,$$

$$\begin{aligned} MW_1(\nu, Q^2) &\rightarrow F_1(x_{bj}), \\ \nu W_2(\nu, Q^2) &\rightarrow F_2(x_{bj}) \end{aligned} \quad (1.2)$$

The parton model predicts that the structure functions at different values of Q^2 but constant x_{bj} should remain the same. This independence from a reference scale is referred to as Bjorken scaling. Experimentally, this gave a signature of scattering off of partons. One could measure the structure functions at different values of Q^2 but the same x_{bj} and if the results were constant then there was visible proof of parton scattering. This scaling was seen to exist as long as one was not in regions of very high or very low x_{bj} , at least over limited ranges of Q^2 .

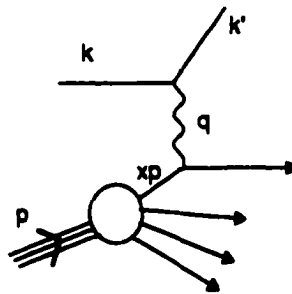


Figure 1.2: The quark parton model of deep inelastic scattering

Now that it had been determined that the proton was made of point-like particles the question remained whether or not these partons corresponded to the quarks theorized by Gell-Mann and Ne'eman to explain hadron spectroscopy. Feynman was able to show that the structure functions of the proton could be described as an incoherent sum of

scatterings off the constituent partons. These partons could be described by the probability distributions of the constituent quarks having a fraction, x , of the parent proton's momenta, $p' = xp$, where p' is the momentum of the parton. The success of this model, known as the quark parton model (QPM), and shown in Fig. 1.1, was showing that the fractional momenta x was equivalent to x_{bj} as Q^2 and $\nu \rightarrow \infty$. This gives us a physical interpretation of the variable x_{bj} .

In the early 1970's it was shown that non-abelian gauge theories had the property of asymptotic freedom. That is at high Q^2 the quarks of quantum chromodynamics (QCD) start behaving as free quarks. If indeed the partons from the QPM were the quarks from QCD, one would have theoretical justification to the assumption of incoherence as $Q^2 \rightarrow \infty$.

The next theoretical advance linking the parton model with QCD came with the inclusion of diagrams with gluon emission by Gribov, Lipatov, Altarelli and Parisi. These higher order effects modify the structure functions so that they no longer strictly scale. That is $F_1(x) \rightarrow F_1(x, Q^2)$. Their predictions for violations of Bjorken scaling in structure functions due to gluon emissions was highly successful in describing experimental data at varying values of Q^2 and x . So one has the interesting dichotomy that both scaling and scaling violations have been used as proof that the QPM correctly describes the physical world.

1.2 Interpretation of F_1 and F_2 Using Parton Distributions

With the question of whether or not the proton has structure out of the way, one can turn to the form of the individual parton distributions within the proton. The relationship between the structure functions $F_{1,2}$ and the constituent parton distributions is

$$2xF_1(x) = F_2(x) = \sum_i e_i^2 x G_{i/p}(x) \quad (1.3)$$

where $G_{i/p}(x)$ is the distribution function of the individual parton of flavor i within the proton. $G_{i/p}(x)dx$ is the probability of finding a quark of flavor i in the range x to $x + dx$.

One can also write

$$G_{i/p}(x) = \frac{dN_{i/p}}{dx}, \quad (1.4)$$

where $N_{i/p}$ is the number of quarks of flavor i in the proton.

The individual quark and gluon distributions are defined as

$$\begin{aligned} u(x) &\equiv G_{u/p}(x), & \bar{u}(x) &\equiv G_{\bar{u}/p}(x), \\ d(x) &\equiv G_{d/p}(x), & \bar{d}(x) &\equiv G_{\bar{d}/p}(x), \\ s(x) &\equiv G_{s/p}(x), & \bar{s}(x) &\equiv G_{\bar{s}/p}(x), \\ & & g(x) &\equiv G_{g/p}(x) \end{aligned} \quad (1.5)$$

Writing $F_2(x)$ out explicitly in terms of the individual quark distributions and neglecting the contributions of charm and heavier quarks

$$\frac{1}{x}F_2^{ep} = \frac{4}{9}[u(x) + \bar{u}(x)] + \frac{1}{9}[d(x) + \bar{d}(x) + s(x) + \bar{s}(x)] \quad (1.6)$$

where the ep superscript denotes electron scattering off of a proton target. Using isospin symmetry one can relate the distributions from the proton with those from the neutron. The proton's $u(x)$ distribution should be equal to the neutron's $d(x)$ distribution and the proton's $d(x)$ should be equal to the neutron's $u(x)$ distribution. The sea quark and gluon distributions are assumed to be equal in the proton and the neutron. The structure function for a neutron target can then be written as

$$\frac{1}{x}F_2^{en} = \frac{4}{9}[d(x) + \bar{d}(x)] + \frac{1}{9}[u(x) + \bar{u}(x) + s(x) + \bar{s}(x)]. \quad (1.7)$$

It should be noted that these functions do have Q^2 dependence due to Altarelli-Parisi gluon emissions

1.3 Polarized Structure Functions

Up until this point all of the equations that I have been giving have been for the unpolarized case. Specifically, $W_{\mu\nu}$ had just terms symmetric in μ and ν . There are also antisymmetric terms dependent on the spin structure of the proton. We write the antisymmetric portion of the hadronic tensor as

$$W_{\mu\nu}^{(A)} = \frac{1}{2}(W_{\mu\nu} - W_{\nu\mu}) = \frac{i}{M^2} \epsilon_{\mu\nu\rho\sigma} Q^\rho \times [S^\sigma (G_1(\nu, Q^2) + \frac{\nu}{M} G_2(\nu, Q^2)) - \frac{1}{M^2} (S \cdot q) p^\sigma G_2(\nu, Q^2)] \quad (1.8)$$

where S_μ is the polarization vector of the nucleon and may be written as

$$S_\mu = \left(\frac{\mathbf{p} \cdot \boldsymbol{\xi}}{M}, \boldsymbol{\xi} + \frac{(\mathbf{p} \cdot \boldsymbol{\xi}) \mathbf{p}}{M(E + M)} \right) \quad (1.9)$$

with $\boldsymbol{\xi}$ being a unit three-vector pointing in the direction of the polarization in some frame. The functions $G_{1,2}$ scale under the QPM and become functions of x just as $W_1(\nu, Q^2) \rightarrow F_1(x)$.

$$\begin{aligned} \frac{\nu}{M} G_1(\nu, Q^2) &\rightarrow g_1(x), \\ \frac{\nu^2}{M^2} G_2(\nu, Q^2) &\rightarrow g_2(x). \end{aligned} \quad (1.10)$$

Again gluon emission diagrams would add a Q^2 dependence to these polarized structure functions.

It also becomes necessary to define the polarized distribution of a parton. The polarized distributions are the difference between the distributions with the helicity pointing in the same direction as the helicity of the proton and with the helicity pointing opposite the helicity of the proton.

$$\Delta q_i(x) = q_i \uparrow(x) - q_i \downarrow(x) \quad (1.11)$$

1.4 Outline of the Thesis

The discussion so far has been centered on deep inelastic scattering, $ep \rightarrow e'X$. The rest of the thesis concentrates on using pion photoproduction, $\gamma p \rightarrow \pi X$, as a means of measuring the parton distribution functions. This is an example of a semi-exclusive process, where some but not all hadrons in the final state are measured. We also include calculations relating semi-exclusive photoproduction to electroproduction, $ep \rightarrow \pi X$.

There are three regions of interest that will be covered. The regions of highest k_T are useful in measuring the the polarized quark distribution functions. Regions of intermediate k_T are useful for measuring the polarized gluon distribution function, Δg . Regions of low k_T are dominated by soft processes whose most important function is to determine the scale at which pQCD becomes a viable method of calculation.

In Chapter 2 I introduce direct meson production, where the pion produced comes from short range processes and is fully calculable within pQCD, as a means of measuring the polarized quark distributions.

Chapter 3 adds extra sophistication to the direct process calculation of chapter two, such as introducing masses and using a full Weizsacker-Williams form for the photon energy distribution. It also adds two mechanisms for producing mesons. The first is producing mesons via fragmentation of quarks and gluons. This mechanism is important because it is highly susceptible to the polarized gluon distributions at leading order. The second mechanism is the resolved photon process, which will be shown to be negligible at the kinematics that we are interested in.

In Chapter 4 the effects of non pQCD background processes in pion photoproduction. Processes such as vector meson dominance are calculated and shown to be important at the kinematics of current experiments.

In Chapter 5, I show how the direct process can be used to probe an analog of

Bloom-Gilman duality for semi-exclusive processes at CEBAF energies.

Chapter 2

Probing polarized parton distributions with meson photoproduction

2.1 Motivation

This chapter describes a flavor sensitive tool for measuring polarized quark distributions, namely photoproduction off nucleons of mesons with high transverse momentum, using polarized initial states.

Known methods such as coincidence measurements of $\vec{\ell} \vec{p}(\vec{d}) \rightarrow \ell \pi^\pm X$ with a proton or deuteron target, give different linear combinations of up and down quark polarized distributions, allowing a flavor decomposition without further theoretical input [2]. The process we will discuss, $\vec{\gamma} \vec{p} \rightarrow M X$ (where the photon is real, targets other than protons are possible, and M is a meson), gives a complementary way to find the polarized quark distributions. The perturbative QCD used in the analysis is justified on the basis of high

meson transverse momentum, rather than by high virtuality of an exchanged photon, and the experiment is a single arm experiment rather than a coincidence one. Good data can in fact come as a by-product of a g_1 experiment since the detectors that measure the final electron or muon can also pick up charged hadrons; recall that if the final lepton is not measured, the form of the cross section ensures that the virtuality of the exchanged photon will be rather low on the average. There is also the possibility of dedicated experiments. The NA59 collaboration at CERN has proposed using crystals as a quarter wave plate to produce circularly polarized photons with energies from 96 to 144 GeV [3].

In Fig. 2.1 I illustrate one of the processes for producing a pion at short distances. Hereafter, I will refer to this type of production as "direct" (The word "direct" was used with a similar meaning in a $\pi N \rightarrow \gamma^* X$ context by Brodsky and Berger long ago [21].) It should be noted that other authors use the term "direct" to refer to direct fragmentation production, Fig 3.2. I shall always refer to that process as fragmentation.

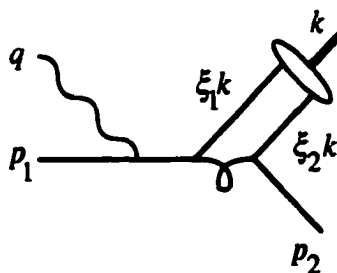


Figure 2.1: One lowest order perturbative diagram for direct photoproduction of mesons from a quark. There are four diagrams total, corresponding to the four places a photon may be attached to a quark line.

Direct processes are amenable to perturbative QCD calculation [4, 5] and produce mesons that are kinematically isolated in the direction they emerge. There are several important features of the direct process that should be emphasized.

One important feature is that the momentum fraction of the active quark is immediately obtainable from experimentally measurable quantities. This is analogous to deep inelastic lepton scattering, where experimenters can measure Q^2 and ν and determine the quark momentum fraction by $x = Q^2/2m_N\nu$. In the present case, the Mandelstam variables are defined using p , q , and k , the momenta of the proton (or other target hadron), the photon, and the meson, respectively,

$$\begin{aligned} s &= (p+q)^2, \\ t &= (q-k)^2, \\ u &= (p-k)^2. \end{aligned} \tag{2.1}$$

These are all experimentally measurable quantities. Neglecting masses, it is easily shown that

$$x = \frac{-t}{s+u}. \tag{2.2}$$

The second important feature is that the polarization asymmetry of meson production is easily calculated at the subprocess level. For example, if R and L represent photon helicities and \pm represent quark helicities, then one polarization asymmetry is

$$\hat{E} \equiv \frac{\frac{d\hat{\sigma}_{R+}}{d\hat{t}} - \frac{d\hat{\sigma}_{R-}}{d\hat{t}}}{\frac{d\hat{\sigma}_{R+}}{d\hat{t}} + \frac{d\hat{\sigma}_{R-}}{d\hat{t}}} = \frac{\hat{s}^2 - \hat{u}^2}{\hat{s}^2 + \hat{u}^2}, \tag{2.3}$$

where the carets represent subprocess quantities. (I should emphasize again that internal quantities such as \hat{s} or \hat{u} are all determinable from experimentally measurable quantities if the direct meson production is dominant.) The measured asymmetry then measures what fraction of the quarks have the same or opposite polarization, for a measured x , as the parent proton.

The third important feature of direct meson production is that changing the flavor of the meson observed changes the flavor of the quarks that the measurement is sensitive to.

For example, when observing a π^+ , only the u and \bar{d} quarks will contribute. In addition, when in the region where valence quarks dominate, formulas can be as simple as

$$\Delta u(x, \mu^2) = u(x, \mu^2) \frac{E}{\hat{E}}, \quad (2.4)$$

where E is the measured polarization asymmetry, \hat{E} is the calculated polarization asymmetry at the quark level, $u(x, \mu^2)$ is the by now relatively well known unpolarized quark distribution for the up quark, μ^2 is a renormalization scale pertinent for the process and kinematics at hand, and Δu is the polarized quark distribution that one wants to measure.

With sensitivity to jets, one can get similar information from the fragmentation process, that is, from subprocesses producing quark and gluon final states with fragmentation turning the quarks and gluons into jets. This has the advantage of having a larger cross section overall. However, if one has data with a single hadron measured (perhaps as a by-product of a single arm deep inelastic lepton scattering experiment), then concentrating on the region where the direct process dominates will yield the information about the quark distributions in the target. And of course, flavor identification is easier for a single hadron than for a jet.

2.2 Calculations

At the subprocess level the direct production of mesons proceeds as in Fig. 2.1. For the case that the incoming photon is circularly polarized and target quark is longitudinally polarized, one gets to lowest order

$$\begin{aligned} \frac{d\hat{\sigma}(\gamma q \rightarrow M q')}{dt} &= \frac{128g_F^2 \pi^2 \alpha \alpha_s^2}{27(-t)\hat{s}^2} I_M^2 \left(\frac{e_q}{\hat{s}} + \frac{e_{q'}}{\hat{u}} \right)^2 \\ &\times [\hat{s}^2 + \hat{u}^2 + \lambda h (\hat{s}^2 - \hat{u}^2)], \end{aligned} \quad (2.5)$$

where λ is the helicity of the photon, h is twice the helicity of the target quark, and g_F is

a flavor factor from the overlap of the $q\bar{q}'$ with the flavor wave function of the meson. It is unity for most mesons if the quark flavors are otherwise suitable; for example

$$g_F = \begin{cases} 1/\sqrt{2} & \text{for } \pi^0 \\ 1 & \text{for } \pi^+ \end{cases}. \quad (2.6)$$

The integral I_M^2 is given in terms of the distribution amplitude of the meson

$$I_M = \int \frac{d\xi_1}{\xi_1} \phi_M(\xi, \mu^2). \quad (2.7)$$

It is precisely the same integral that appears in the perturbative calculation of the π^\pm electromagnetic form factor or of the $\pi^0\gamma\gamma$ form factor. Finally,

$$\begin{aligned} \hat{s} &= (p_1 + q)^2, \\ \hat{u} &= (p_1 - k)^2, \end{aligned} \quad (2.8)$$

and \hat{t} is the same as t .

The helicity dependent asymmetry at the subprocess level may be immediately read off and is given in Eqn. (2.9). The notation “ E ” comes from pion photoproduction work (see for example [6]); it is analogous to C_{LL} or A_{LL} in pp collision studies.

$$\hat{E} \equiv \frac{\frac{d\hat{\sigma}_{R+}}{d\hat{t}} - \frac{d\hat{\sigma}_{R-}}{d\hat{t}}}{\frac{d\hat{\sigma}_{R+}}{d\hat{t}} + \frac{d\hat{\sigma}_{R-}}{d\hat{t}}} = \frac{\hat{s}^2 - \hat{u}^2}{\hat{s}^2 + \hat{u}^2}, \quad (2.9)$$

Another possibly useful asymmetry is the single polarization asymmetry, where the photon has linear polarization either in or normal to the plane defined by the outgoing meson. This asymmetry is (using $\hat{\sigma}$ for $d\hat{\sigma}/d\hat{t}$)

$$\hat{\Sigma} = \frac{\hat{\sigma}_{\parallel} - \hat{\sigma}_{\perp}}{\hat{\sigma}_{\parallel} + \hat{\sigma}_{\perp}} = \frac{2\hat{s}\hat{u}}{\hat{s}^2 + \hat{u}^2}. \quad (2.10)$$

It is interesting to note that \hat{E} is the same as one would obtain for Compton scattering, $\gamma q \rightarrow \gamma q$, off the quark.

Within a hadron target, the quark has light cone momentum fraction x , and $p_1 \simeq xp$.

Neglecting masses, one has

$$\hat{s} + \hat{t} + \hat{u} = 0. \quad (2.11)$$

Still neglecting masses, one has that

$$\hat{s} = xs, \quad \hat{t} = t, \quad \hat{u} = xu. \quad (2.12)$$

Hence the earlier quoted equation (2.2) giving x in terms of measurable quantities follows.

To the overall process, the direct subprocess makes a contribution that requires no integration to evaluate,

$$\begin{aligned} E_\pi \frac{d\sigma}{d^3k} &= \frac{sx^2}{\pi(-t)} \frac{d\sigma(\gamma p \rightarrow M + X)}{dx dt} \\ &= \frac{sx^2}{\pi(-t)} \sum_q G_{q/p}(x, \mu^2) \frac{d\hat{\sigma}(\gamma q \rightarrow Mq')}{dt}, \end{aligned} \quad (2.13)$$

where the helicity summations are tacit.

The helicity dependent asymmetry is reduced from its subprocess value because not all the quarks in a hadron have the same polarization as the hadron does. This is what allows us to measure the polarized quark distributions. Take π^+ production off a proton target as an example. The initial active quark may be either a u or a \bar{d} , and

$$\begin{aligned} E(x, u/s) &= \hat{E}(u/s) \\ &\times \frac{\left(\frac{\epsilon_u}{s} + \frac{\epsilon_d}{u}\right)^2 \Delta u(x) + \left(\frac{\epsilon_d}{s} + \frac{\epsilon_u}{u}\right)^2 \Delta \bar{d}(x)}{\left(\frac{\epsilon_u}{s} + \frac{\epsilon_d}{u}\right)^2 u(x) + \left(\frac{\epsilon_d}{s} + \frac{\epsilon_u}{u}\right)^2 \bar{d}(x)}. \end{aligned} \quad (2.14)$$

I have let

$$q(x) = q(x, \mu^2) = G_{q/p}(x, \mu^2) \quad (2.15)$$

for the unpolarized distributions, and

$$\Delta q(x) = \Delta q(x, \mu^2) = G_{q+/p+} - G_{q-/p+}(x, \mu^2). \quad (2.16)$$

Also, because of the ratio, the formula can be written in terms of the measured s and u directly rather than using the subprocess variables. At higher x , where the valence quarks dominate, one may drop the \bar{d} terms in the above expression and obtain the simple result (2.4) quoted earlier.

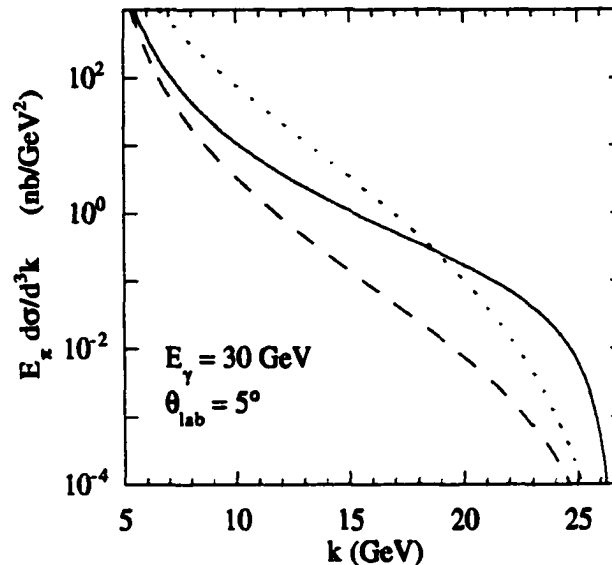


Figure 2.2: Comparing direct and fragmentation photoproduction of π^+ off protons, for $E_\gamma = 30$ GeV and $\theta_{lab} = 5^\circ$. The solid line is direct production of π^+ and the dotted line is fragmentation production of π^+ . For reference, the dashed line shows direct production of π^0 . The abscissa is $k = |\vec{k}|$ in the lab.

Regarding the relevance of the direct process and its relation to the values of x that are probed, the direct process is higher twist, and does not generally dominate the production of mesons. It does dominate in the region of very high transverse momentum. The main competition is the fragmentation process, where the observed meson is part of a jet. The fragmentation process tails off at the highest transverse momenta simply because of its implicit requirement that one meson take all or nearly all the momentum

of the quark is unlikely to be satisfied in a jet. For illustration, a calculation comparing direct to fragmentation photoproduction of π^+ 's off a proton is shown in Fig. 2.2, based on calculations by Carlson and Wakely [4], and using the asymptotic distribution amplitude for the pion (using the Chernyak-Zhitnitsky distribution amplitude would make the direct process calculation larger by a factor 25/9). This particular example is for photon energy 30 GeV with the pion emerging at 5° in the lab. The direct process is larger than the fragmentation process for pion momenta above 20 GeV; this corresponds to x above about 0.24. Generally, if the meson can be produced from a valence quark in the target, the region in which the direct process dominates will correspond to values of x within the valence region.

2.3 Results

The chief question must be how sensitive a measurement of Δq can be made. To study this question, I use three different models or fits to the polarized quark distributions. These are the fits of Gehrmann and Stirling (GS) [7], of Glück, Reya, Stratmann, and Vogelsang (GRSV) [8], and a suggestion of Soffer *et al.* [9]. All fit the available data on g_1 from deep inelastic lepton scattering experiments. For the first two, the renormalization scale dependent results for the polarized parton distributions was obtained directly from the authors. The Soffer *et al.* suggestion relates the polarized and unpolarized distribution functions, specifically,

$$\begin{aligned}\Delta u(x) &= u(x) - d(x), \\ \Delta d(x) &= -\frac{1}{3}d(x),\end{aligned}\tag{2.17}$$

and other polarized distributions are treated as small. When using the Soffer *et al.* suggestion, it is teamed with the CTEQ [10] quark distributions. In all cases, the renormalization

scale μ^2 is set to k_T^2 , where k_T is the transverse momentum of the produced meson.

The upper part of Fig. 2.3 shows the asymmetry, E , for π^+ photoproduction off protons. (Both Fig. 2.3 and 2.3 are for 100% polarization of the beam and target.) Notice that the asymmetries are significant, and that the GS and GRSV polarized distributions give about the same result, but the Soffer *et al.* suggestion gives an asymmetry that is significantly larger. The other part of Fig. 2.3 shows the π^- case. The asymmetry has the opposite sign because now the d valence quark dominates, and in all the models the u is polarized along the direction of the proton while the d is opposite. For the π^- , it is the GRSV and Soffer *et al.* results that are about the same, and the GS is significantly different and usually larger in magnitude.

Electroproduction with the final electron unobserved is much akin to photoproduction. Single arm electroproduction experiments commonly get such data when a charged hadron rather than an electron triggers the detector. The form of the cross section ensures that low Q^2 events dominate if Q^2 is not measured.

Hence electroproduction with just the single hadron observed usually has the photon nearly on shell, but only the upper and lower limits of the photon energy are known. The three models for the polarized quark distributions still give distinguishable predictions, as I shall show. For a given electron energy E_e , the photon energy spectrum is given fairly accurately by

$$\frac{dN_\gamma}{dE_\gamma} \propto \frac{1}{E_\gamma} \quad (2.18)$$

up to close to the cutoff at $E_\gamma = E_e$. The polarization of the photon is nearly the polarization of the electron provided the photon takes most of the electron's energy. Polarization details can be found in [11]; most usefully, if P_γ and P_e are the circular and longitudinal

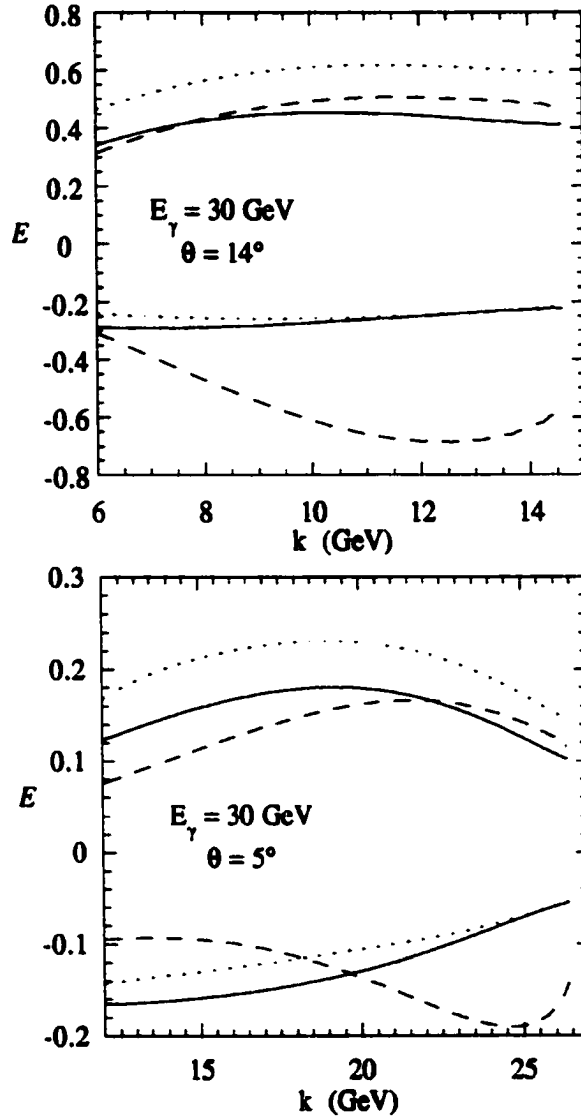


Figure 2.3: The upper three curves are the helicity dependent asymmetries for π^+ photoproduction off the proton, for 30 GeV photons and lab angle 5 or 14° . The solid line is for the GRSV polarized quark distributions; the dashed line is for GS; and the dotted line is for the suggestion of Soffer *et al.* GRSV is about the same as GS for the π^+ case. The lower three curves are for π^- photoproduction. GRSV and GS are well separated in the π^- case.

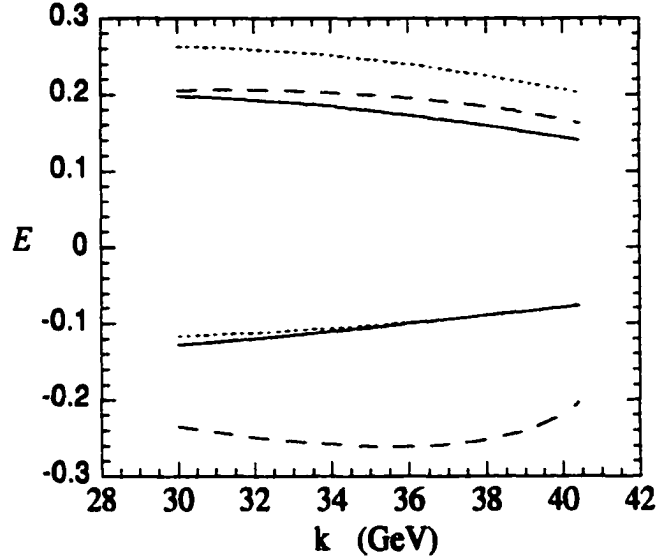


Figure 2.4: Polarization asymmetry results for 50 GeV incoming electrons, with pions emerging at 5° lab angle and the electrons not observed. We have integrated over the energies and polarizations of the virtual (but on the average low Q^2) photons with weightings as indicated in the text. The upper three curves are for the π^+ and the lower three curves are for the π^- . The solid, dashed, and dotted lines are for GRSV, GS, and Soffer *et al.*, respectively.

polarizations of the photon and electron, respectively, then

$$\frac{P_\gamma}{P_e} = \frac{y(4-y)}{4-4y+3y^2}. \quad (2.19)$$

where $y = E_\gamma/E_e$.

Fig. 2.3 shows polarization asymmetry results for 50 GeV incoming electrons, with pions emerging at 5° lab angle and photon energies and polarizations weighted as indicated above. Despite the weighted average over photon energies, the models still give different predictions.

Another possibility for producing real photons with circular or linear polarization is the laser backscattering technique [12].

2.4 Discussion

A number of questions may be asked about the applicability of perturbative QCD. I could of course point out that due to the dependence on ratios of cross sections, many potential problems may cancel out. However, I shall address some of the questions more directly.

One simple question is whether the “ X ” in $\gamma + p \rightarrow M + X$ is out of the resonance region. Letting m_X be the mass of the collection of particles X , one should require $m_X > 2$ GeV, and neglecting the mass of the meson one has

$$m_X = \sqrt{s + t + u - m_N^2}. \quad (2.20)$$

For $E_\gamma = 30$ GeV and $\theta_{lab} = 5^\circ$, the requirement becomes $k < 25$ GeV, which is easy to satisfy. Lower energies could be more troublesome. At 12 GeV incoming photon energy, with a π^+ exiting at 22° , the requirements of dominance of the direct process and of being out of the resonance region just leave a window $4.8 < k < 5.3$ GeV, corresponding to $0.62 < x < 0.74$.

Another question regards higher twist corrections, for example, corrections due to the quarks in the pion having finite momentum transverse to the pion’s overall momentum. This has been much studied in the context of the pion electromagnetic form factor [13]. As has been remarked, the integral over the pion’s distribution amplitude that appears here is the same as appears in the pion form factor. However [4], the momentum transfer scale as judged by how far the transferred gluon is off shell is much larger in pion photoproduction than in the pion form factor. To be more definite, if the photon attaches to the produced $q\bar{q}$ pair in Fig. (5.13) the gluon is off shell on the average by

$$\langle q_G^2 \rangle = \langle \xi_2 \rangle x u, \quad (2.21)$$

The corresponding quantity if the photon attaches to the initial quark is larger, though

timelike. The average ξ_2 is weighted by the integrand of I_π and is $1/3$ and $1/5$ for the asymptotic and Chernyak-Zhitnitsky distribution amplitudes, respectively. The pion electromagnetic form factor involves the distribution amplitude twice, and if the virtual photon is off shell by an amount Q^2 , then the gluon in that process is off shell by

$$\langle q_G^2 \rangle = -\langle \xi_2 \rangle^2 Q^2. \quad (2.22)$$

Matching the gluon virtualities, there is a correspondence

$$Q^2 \leftrightarrow \frac{x(-u)}{\langle \xi_2 \rangle}. \quad (2.23)$$

This means that for the case of incoming 30 GeV photons and pions out at 5° , in the region of direct process dominance and above the resonance region, the integrals over the distribution amplitude are the same as those for $F_\pi(Q^2)$ with

$$15 \text{ GeV}^2 < Q^2 < 80 \text{ GeV}^2. \quad (2.24)$$

Thus higher twist effects will be less significant for measurable photoproduction of high transverse momentum mesons than for meson form factors at any currently measured momentum transfers.

Perturbative corrections that are higher order in α_s have not been calculated. They may be calculated along the lines of [14] for the $\pi^0\gamma\gamma$ and or of [15] for the π^\pm electromagnetic form factors. For both of these, using the asymptotic distribution amplitude and a suitable choice of renormalization scale, the magnitude of the correction was about 20%, decreasing the $\pi^0\gamma\gamma$ and increasing the π^\pm form factors.

Regarding the single polarisation asymmetry Σ , for the direct process, it is always negative and for forward center of mass angles it is large in magnitude. As one moves to lower k and the fragmentation process becomes more important, there is a significant dilution of Σ . The reduction of Σ occurs because the $\gamma\gamma$ fusion process becomes important,

and Σ for that process is precisely zero. If Σ is observed and seen to be large, it is one sign that the direct process is important. For instance, for the same E_γ and θ_{lab} as above, the value of Σ at $k = 22$ GeV is -0.61 , -0.94 , and -0.86 , respectively, for the fragmentation alone, the direct process alone, and their properly weighted total (using the Soffer *et al.* model).

I believe that photoproduction of high transverse momentum mesons is an accurate and flavor sensitive way to measure the polarized quark distributions in the valence region.

Chapter 3

Measuring polarized gluon and quark distributions with meson photoproduction

3.1 Motivation

In this chapter, I will discuss photoproduction of high transverse momentum pions from polarized initial states. There are three motivations for doing so. One is the opportunity to learn the polarization distribution of quarks and gluons in nucleons. I will show that pion photoproduction with polarized initial states has, over a wide kinematic region of moderate transverse momentum pions, a large sensitivity to the polarized gluon distribution functions of the target. Within this wide kinematic region there are broad circumstances where the known polarized quark distributions all give similar pion photoproduction contributions, so that differences among the results are due mainly to the polarized gluon distributions. Hence data where rather ordinary mesons are produced can select among the

various models for this quantity.

The last chapter covered the kinematic region of very high transverse momentum pions where the gluon contributions are small but the differences among the various models for the polarized quark distributions are significant. Hence examining different kinematic regions of pion photoproduction yields information about both polarized quark and polarized gluon distributions.

A third motivation, also dependent upon the highest transverse momentum pions, is the possibility of learning something about the pion distribution amplitude. In this region, ratios of cross sections determine the target's quark distributions, but the magnitude of the cross section depends upon the same integral involving the pion distribution amplitude that enters the pion electromagnetic form factor of the $\pi^0\gamma\gamma^*$ vertex. Hence if one looks at the unpolarized case, where the target distributions are fairly well known, one has another measure of this integral. (Pion photoproduction in the unpolarized case has been well and successfully studied theoretically and experimentally [18], but not at the highest transverse momenta where the pions will be dominantly produced in a short distance process rather than via fragmentation [4, 5, 17].)

Polarized gluon distributions are not well determined at present. Something is learned from [7, 8, 19, 20] the measurements of g_1 , but gluons contribute to g_1 only in higher order or through their effects upon the evolution of the polarized quark distributions. The analyses of g_1 can be abetted by perturbative QCD considerations at high x [20]. Overall, however, the present constraints upon the polarized gluon distributions are not great and there is a large variance among $\Delta g(x, \mu^2)$ models, as may be seen in Fig. 3.1.

The process I discuss, $\vec{\gamma} \vec{p} \rightarrow \pi X$ (where the photon is real and targets other than protons are possible), gives a complementary way to find the polarized quark distributions and is sensitive to the gluon distributions in leading order. The perturbative QCD that

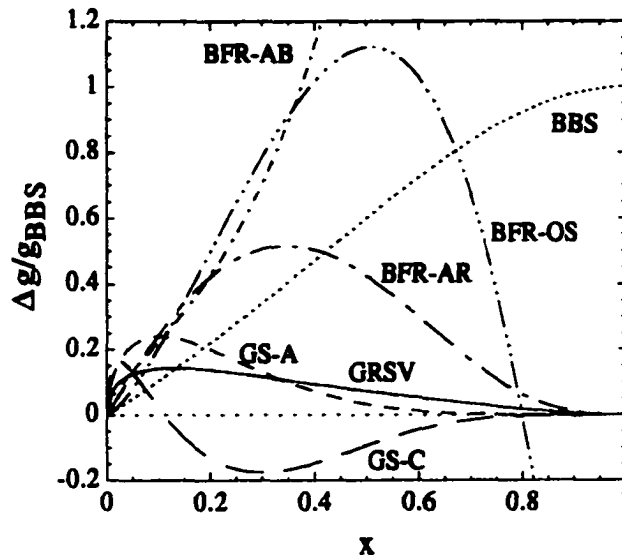


Figure 3.1: A number of polarized gluon distributions, all normalized to the unpolarized BBS gluon distribution. The sources of these distributions are given later in the text.

used in the analysis is justified on the basis of high meson transverse momentum.

There are several processes that produce pions. At the highest transverse momenta, mesons are produced by short range processes illustrated in Fig. 2.1. I call these direct processes because the photon interacts directly with the target partons and also the pion is produced immediately.

At moderate pion transverse momentum, the main process is one I call the fragmentation process. The photon does interact directly with the partons of the target, but the meson is produced by fragmentation of one of the final state quarks or gluons. This time, an integration is needed to calculate the cross section, but any given model makes a definite prediction that can be compared to data. Unlike the case for g_1 , interactions involving the gluons in the target contribute to the cross section in lowest order. One of the important

subprocesses is photon-gluon fusion, $\gamma + g \rightarrow q + \bar{q}$. The polarization asymmetry of this process is very large. Indeed, neglecting masses, it is -100% : the process only goes if the photon and gluon have opposite helicity. Hence this process is even more significant for the polarization asymmetry than it is to the total cross section. There are situations where the results excluding the gluon polarization are close to the same for all the modern parton distribution function models or parameterizations. Then the differences among the results from different models are due to the polarized gluon distributions, and the differences over the spectrum of available models are large. Hence, the data will adjudicate among the different suggest polarized gluons distributions.

There is also the resolved photon process, where the photon turns into hadronic material before interacting with the target. However, for the kinematic situations highlighted, the resolved photon contributions are below both the fragmentation and direct contributions.

Calculational details are outlined in the following section. Some results and tests of the calculations are outlined in the next following section. Section 3.4 shows results involving polarized initial states, in particular showing how sensitive the results are the the different models for the polarized parton distributions and how well they could be extracted from the data. Some conclusions will be given in section 3.5.

3.2 Calculations

There are three categories of processes that contribute to pion photoproduction; fragmentation processes, direct processes, and resolved photon processes.

Fragmentation processes have quarks and gluons produced in short range reactions followed by fragmentation at long distances of either a quark or a gluon to produce the observed pion. The short distance part of the process is perturbatively calculated and

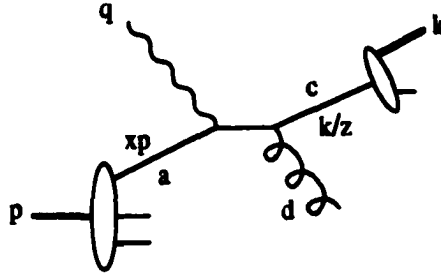


Figure 3.2: One diagram for photoproducing π mesons via fragmentation.

the long distance part is parameterized as a fragmentation function for partons into pions. Direct processes, in my nomenclature, occur when the pion is produced in a short range reaction via a radiated gluon giving a quark-antiquark pair, one of which joins the initial quark to produce the pion. This process is perturbatively calculable, given the distribution of initial quarks, and produces isolated pions rather than pions as part of a jet. The direct process can dominate the fragmentation process for very high transverse momentum pions. Resolved photon processes are photons fluctuating into hadrons, most simply a quark-antiquark pair, which then interact with the partons of the target. The resolved photon processes can be important for high initial energy, especially for pions produced backward in the center of mass.

Fragmentation processes, of which one example is shown in Fig. 3.2, are important over a wide range of kinematics for the present paper, and I start by recording the relevant formulas [16]. In general, if the photon interacts directly with a constituent of target N but the pion is produced as part of a jet,

$$\sigma = \sum_{a,c,d} \int G_{a/N}(x) \frac{d\hat{\sigma}}{d\hat{t}}(\gamma + a \rightarrow c + d) D_{\pi/c}(z) dx d\hat{t} dz. \quad (3.1)$$

Here, x is the ($\sigma = \sum_{a,c,d} \int G_{a/N}(x) \frac{d\hat{\sigma}}{d\hat{t}}(\gamma + a \rightarrow c + d) D_{\pi/c}(z) dx d\hat{t} dz$: the struck parton a ,

z is the fraction of the parton c 's momentum that goes into the pion, and \hat{s} , \hat{t} , and \hat{u} are the Mandelstam variables for the subprocess $\gamma + a \rightarrow c + d$. The scale dependence of the parton distribution functions G and the fragmentation functions D will often be tacit, as it is above. As a differential cross section for the pion, one gets

$$E_{\pi} \frac{d\sigma}{d^3k} = \frac{s - m_N^2}{-\pi t} \sum_{a,c,d} \int_{z_{\min}}^1 \frac{dz}{z} x^2 \times G_{a/N}(x) \frac{d\hat{\sigma}}{d\hat{t}}(\gamma + a \rightarrow c + d) D_{\pi/c}(z), \quad (3.2)$$

The Mandelstam variables for the overall process s , t , and u are defined for the inclusive process by

$$\begin{aligned} s &= (p + q)^2 \\ t &= (q - k)^2 \\ u &= (p - k)^2 \end{aligned} \quad (3.3)$$

where q , p , and k are the momenta of the incoming photon, the target, and the outgoing pion, respectively. The lower integration limit is

$$z_{\min} = -\frac{t + u - m_N^2}{s - m_N^2}, \quad (3.4)$$

and

$$x = \frac{-t}{z(s - m_N^2) + (u - m_N^2)}. \quad (3.5)$$

When the target and projectile are polarized, I define

$$\Delta\sigma = \frac{1}{2} (\sigma_{R+} - \sigma_{R-}), \quad (3.6)$$

where R and L represent photon helicities and \pm represent target helicities, and similarly for $\hat{\sigma}$. Also, the polarized parton distributions are defined by

$$\Delta G_{a/N}(x) = \Delta G_{a/N}(x, \mu^2) = G_{a+/N+}(x) - G_{a-/N+}(x). \quad (3.7)$$

For quarks and gluons and proton targets I will often use the notation $q(x) \equiv G_{q/p}(x)$ and $g(x) \equiv G_{g/p}(x)$ and their polarized equivalents. The cross section is now given by

$$E_\pi \frac{d\Delta\sigma}{d^3k} = \frac{s - m_N^2}{-\pi t} \sum_{a,c,d} \int_{z_{\min}}^1 \frac{dz}{z} x^2 \times \Delta G_{a/\Lambda}(x) \frac{d\Delta\hat{\sigma}}{d\hat{t}} (\gamma + a \rightarrow c + d) D_{\pi/c}(z). \quad (3.8)$$

The relevant subprocess cross sections are

$$\begin{aligned} \frac{d\hat{\sigma}}{d\hat{t}}(\gamma + q \rightarrow g + q) &= \frac{8\pi e_q^2 \alpha_s}{3\hat{s}^2} \left(\frac{-\hat{s}}{\hat{u}} + \frac{\hat{u}}{-\hat{s}} \right), \\ \frac{d\hat{\sigma}}{d\hat{t}}(\gamma + g \rightarrow q + \bar{q}) &= \frac{\pi e_q^2 \alpha_s}{\hat{s}^2} \left(\frac{\hat{u}}{\hat{t}} + \frac{\hat{t}}{\hat{u}} \right), \\ \frac{d\Delta\hat{\sigma}}{d\hat{t}}(\gamma + q \rightarrow g + q) &= \frac{8\pi e_q^2 \alpha_s}{3\hat{s}^2} \left(\frac{\hat{s}}{-\hat{u}} - \frac{\hat{u}}{-\hat{s}} \right), \\ \frac{d\Delta\hat{\sigma}}{d\hat{t}}(\gamma + g \rightarrow q + \bar{q}) &= -\frac{\pi e_q^2 \alpha_s}{\hat{s}^2} \left(\frac{\hat{u}}{\hat{t}} + \frac{\hat{t}}{\hat{u}} \right). \end{aligned} \quad (3.9)$$

The cross section for $\gamma + q \rightarrow g + q$ is written for \hat{t} being the momentum transfer between the photon and the gluon. The asymmetry for the quark target is positive and the asymmetry for the gluon target is -100% .

The direct process was the focus of the preceding chapter and the relevant formulas can be found there. I will make some comments on this process here.

The direct process is higher twist, nominally suppressed by a factor of scale f_π^2/s . However, for very high transverse momentum pions it is the dominant production process. When it is the dominant process, one can take advantage of the nice feature that the momentum fraction x of the struck quark is completely determined by experimentally measurable quantities. With $p_1 \simeq xp$ and estimating mass corrections with a proportional mass approximation, one has

$$\hat{s} + \hat{t} + \hat{u} = 2x^2 m_N^2. \quad (3.10)$$

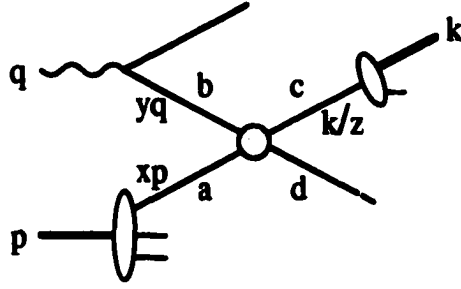


Figure 3.3: A resolved photon process.

Further,

$$\hat{s} = xs - x(1-x)m_N^2, \quad \hat{t} = t, \quad \hat{u} = xu - x(1-x)m_N^2. \quad (3.11)$$

Hence,

$$x = \frac{-t}{s + u - 2m_N^2}. \quad (3.12)$$

Thus to the overall process, the direct subprocess makes a contribution that requires no integration to evaluate. For the polarized case

$$\begin{aligned} E_\pi \frac{d\Delta\sigma}{d^3k} &= \frac{(s - m_N^2)x^2}{-\pi t} \frac{d\sigma(\gamma p \rightarrow \pi + X)}{dx dt} \\ &= \frac{(s - m_N^2)x^2}{-\pi t} \sum_q \Delta G_{q/p}(x, \mu^2) \frac{d\Delta\hat{\sigma}(\gamma q \rightarrow \pi q')}{dt}, \end{aligned} \quad (3.13)$$

where the helicity summations are tacit. The unpolarized case is the same with the Δ 's.

Just a quick note on the resolved photon contributions. One such contribution is illustrated in Fig. 3.2, where the photon turns into hadrons such as a quark-antiquark pair before interacting with the target. The cross section for such a process has been calculated by Afanasev et al [33]. I will not include the relevant formulas here since the results have been shown to not be significant in the kinematic regions considered in this work.

Good data can come from electroproduction experiments where only the outgoing pion is observed. Because of the q^{-4} in the cross section, the photons are nearly all close

to real, and the equivalent photon approximation gives the general connection between the electroproduction and photoproduction cross sections [25],

$$d\sigma(eN \rightarrow \pi X) = \int_{E_{\min}}^{E_e} dE_\gamma N(E_\gamma) d\sigma(\gamma N \rightarrow \pi X). \quad (3.14)$$

where E_γ is the energy of the photon and

$$N(E_\gamma) = \frac{\alpha}{\pi E_\gamma} \left[\frac{E_e^2 + E_e'^2}{E_e^2} \left(\ln \frac{E_e}{m_e} - \frac{1}{2} \right) + \frac{E_\gamma^2}{2E_e^2} \times \right. \\ \left. \times \left(\ln \frac{2E_e'}{E_\gamma} + 1 \right) + \frac{(E_e + E_e')^2}{2E_e^2} \ln \frac{2E_e'}{E_e + E_e'} \right], \quad (3.15)$$

where $E_e' = E_e - E_\gamma$. The lower limit on the photon energy integral is

$$E_{\min} = \frac{k}{1 - 2(k/m_N) \sin^2(\theta_{\text{lab}}/2)}. \quad (3.16)$$

The polarization details were covered in the last chapter.

I close this section with a few comments on our procedures.

I used $\alpha_s(\mu^2)$ with the renormalization scale set to the pion transverse momentum. Not all of the pieces needed for the calculation are known beyond leading order and I have worked to lowest order throughout. I took $\Lambda_{QCD} = 175$ MeV for four flavors. (This corresponds, to about $\pm 6\%$ in α_s for $\mu = 1 - 5$ GeV, to a four flavor Λ_{QCD} of 295 MeV in the next to leading order formula, which matches to a five flavor Λ_{QCD} of 209 MeV, which is the central value quoted by the Particle Data Group [26]. Uncertainties are roughly ± 40 MeV on the 209 and 175 MeV numbers, and ± 50 MeV on the 295 MeV.)

The mass corrections were estimated using a proportional mass approximation. The parton that came from the target was given a mass xm_N , and the final parton that did not go into the pion was given the same mass. The parton that did go into the pion was treated as massless (like the pion), and the same was done for the parton that came from the photon in the resolved photon process. A fully defensible treatment of mass corrections would

require a solution to QCD. The proportional mass approximation just described has the virtues of being simple and of giving the same kinematic limits from thresholds and energy conservation for the subprocess as for the overall process. Hence, it is an improvement over putting in no mass corrections, though it may be treated largely as a way to receive a warning to be careful when the mass corrections are big. For the situations studied, the mass corrections were not large except when the cross sections were very small.

A discussion on the fragmentation functions used may be found in Appendix A

3.3 Results without Polarization

Our present main interest is on results obtainable for polarized beams and targets. However, both for checking the model and for intrinsic interest I will present some results with no polarization involved. First, Fig. 3.3 shows the relative size of the fragmentation, direct, and resolved photon contributions for some kinematics of interest, namely 50 GeV electrons with the only observed final state particle being a π^+ emerging at 5.5° in the lab.

Commentary on the quark and gluon distribution models used is put in the next section, so that I can bundle the remarks on the polarized and unpolarized distributions into one location.

One sees that the cross section falls quickly with increasing pion momentum. The fragmentation process is the main one at lower pion momenta, and the direct process takes over above about 26 GeV for this particular angle and incoming energy.

In addition, one sees that the resolved photon process is not particularly important here. At higher energies it increases in relative importance [28] and at HERA energies ($\sqrt{s} \approx 300$ GeV), the resolved photon process dominates except for very forward angles. The reason for its fast increase involves the lower average y possible at higher energies, as well as the reduced kinematic constraint upon a three step (three integrals in the calculation)

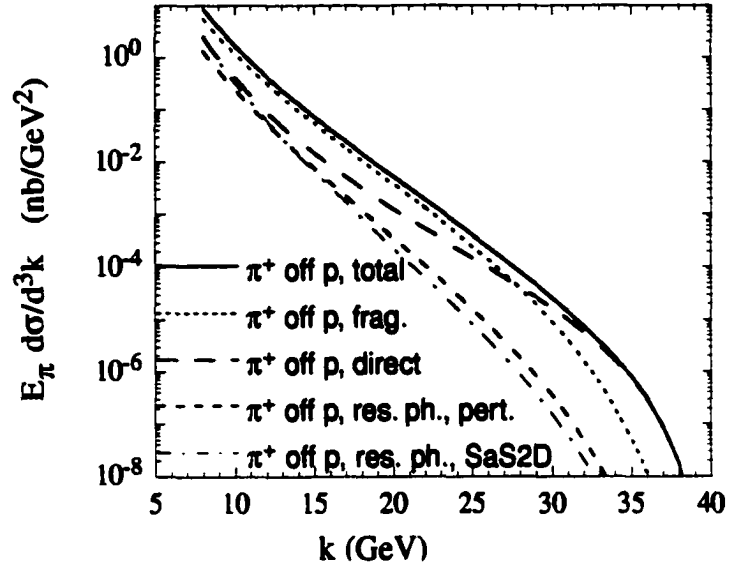


Figure 3.4: Comparing fragmentation, direct, and resolved photon processes for $e + p \rightarrow \pi^+ + X$ with $E_e = 50$ GeV and $\theta_{lab} = 5.5^\circ$. These all use the GRSV parton distributions. The relative size of the contributions should not depend much on which parton distributions used. For the resolved photon contribution [33], the result of both the perturbative splitting function for the photon, and the more sophisticated SaS 2D are shown. Both are small for these kinematics.

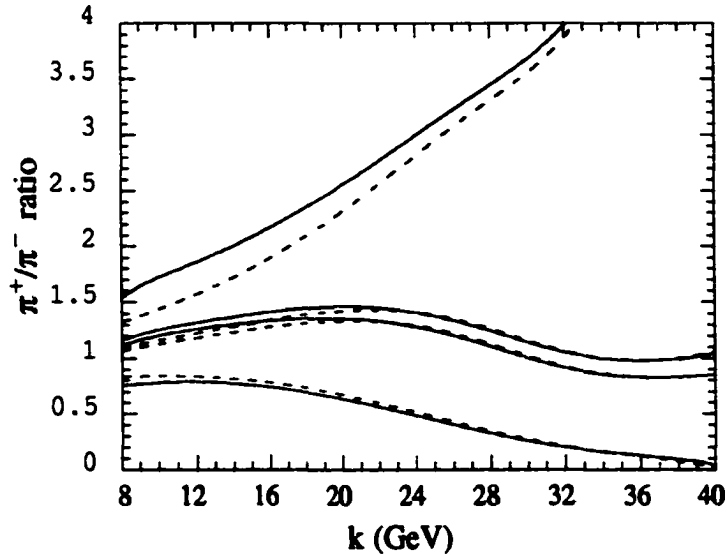


Figure 3.5: The π^+/π^- ratio for $E_e = 50$ GeV and $\theta_{lab} = 5.5^\circ$ for the pions. The dashed curve is for GRV and the solid curve is for CTEQ. Both have $u(x)/d(x) \sim 1/(1-x)$ for large x . The four pairs of curves are for, top to bottom, protons, a target which is 5/9 protons and 4/9 neutrons, an isoscalar target, and neutrons.

process as the energy increases.

The π^+/π^- ratio off proton and neutron targets is shown in Fig. 3.3, again for 50 GeV incoming electrons. Most of the models for the parton distributions lead to the similar results except at the highest k , which will be discussed below. Also included in the figure are two sets of predictions for the π^+/π^- ratio of isoscalar or nearly isoscalar targets. Fig. 3.3 details the π^+/π^- ratio for 50 GeV incident electrons on a target that is 5/9 protons and 4/9 neutrons. (These are relevant numbers for one actual ammonia target, where the nitrogen is ^{15}N and the hydrogens have plain proton nuclei.)

The predictions for the π^+/π^- ratio are different for purely direct and purely fragmentation processes. For an isoscalar target, the ratio is not sensitive to the quark distri-

butions, and the observed behavior of the π^+/π^- ratio could be a clear signal for the direct process taking over from fragmentation with increasing pion momentum. For a proton or neutron target, there is much sensitivity to the quark distributions. The size of $d(x)$ vs. $u(x)$ at high x is one of the remaining open questions for unpolarized quark distributions, and if it can be established that the high x —high k results are mainly direct (or mainly fragmentation, if that should happen against our expectations) then the observed π^+/π^- ratio becomes a direct measure of $d(x)/u(x)$.

To elaborate the preceding remarks, consider what happens for x approaching unity, where only valence quarks matter and π^+ comes from u and π^- comes from d . If fragmentation dominated, then

$$\left. \frac{\pi^+}{\pi^-} \right|_{frag} = 4 \frac{f_p u(x) + (1 - f_p) d(x)}{f_p d(x) + (1 - f_p) u(x)}, \quad (3.17)$$

where the target is fraction f_p proton. The "4," of course, is $(e_u/e_d)^2$. Also, for fragmentation, $u(x)$ and $d(x)$ must be understood as appearing inside some integrals, but only the ratio $d(x)/u(x)$ as $x \rightarrow 1$ will matter here.

For the direct case, the short distance nature of the reaction allows the photon to interact with the produced $q\bar{q}$ pair as well as with the target quark, so it makes less difference whether a π^+ or π^- is produced. One has—see eqn. (??)—,

$$\left. \frac{\pi^+}{\pi^-} \right|_{direct} = \left(\frac{s + 2|u|}{2s + |u|} \right)^2 \frac{f_p u(x) + (1 - f_p) d(x)}{f_p d(x) + (1 - f_p) u(x)}. \quad (3.18)$$

The prefactor is less than one, but approaches one for small angles and maximum pion energy, when $|u| \rightarrow s$.

For isoscalar ($I_3 = 0$ suffices) or nearly isoscalar targets the π^+/π^- ratio would approach 4 for maximum momentum in the fragmentation process, or approach 1 for the direct process, and be rising with momentum. One can qualitatively understand the curve shown for the near isoscalar case in Fig. 3.3: at low k , fragmentation dominates but the

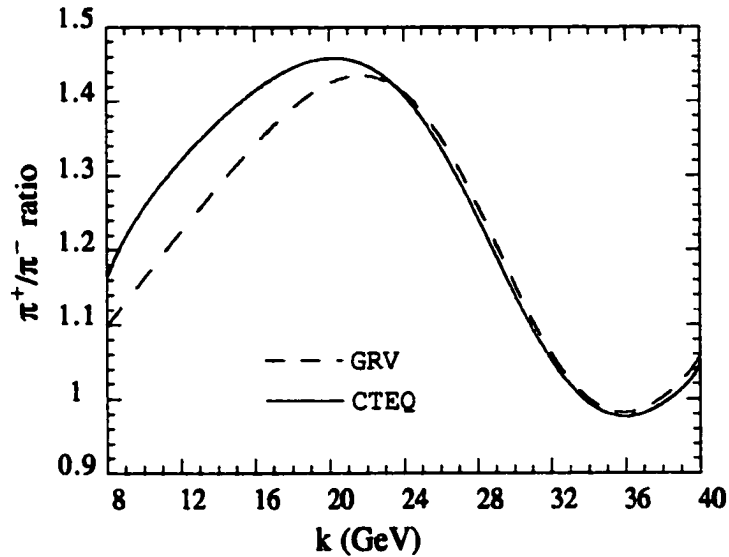


Figure 3.6: Detail of π^+/π^- ratio for $E_e = 50$ GeV and $\theta_{lab} = 5.5^\circ$ for the pions, for a target which is 5/9 protons and 4/9 neutrons.

π^+/π^- ratio is not large as there are important contributions from gluons and sea quarks in the target. As k rises, the valence quark contributions become relatively more important and the ratio rises. Then the direct or short distance process takes over and the ratio falls, and finally rises a bit due to the prefactor in the last equation after the process is almost pure direct.

For a proton target, the $x \rightarrow 1$ limit of the ratio $d(x)/u(x)$ is important. Possibilities include,

$$\frac{d(x)}{u(x)} = \begin{cases} 0 & \text{many fits} \\ 1/5 & \text{pQCD} \\ 1/2 & SU(6) \end{cases} \quad (3.19)$$

Both CTEQ [10] and GRV [29] have $u(x)$ and $d(x)$ falling with different powers of $(1-x)$, with $d(x)$ falling faster, and so are examples of the first category. The BBS [20] distributions,

whose non-separation of q and \bar{q} is inconsequential at high q , do satisfy the pQCD constraint and so give a different π^+/π^- ratio as the pion momentum reaches its maximum.

3.4 Results with Polarization

The asymmetry E (or A_{LL}) for π^\pm photoproduction off both the proton and neutron has been calculated. If R and L represent photon helicities and \pm represent target helicities, then E is defined by

$$E \equiv \frac{\sigma_{R+} - \sigma_{R-}}{\sigma_{R+} + \sigma_{R-}}. \quad (3.20)$$

There is direct sensitivity to the polarized gluon distribution $\Delta g(x, \mu^2)$ since at moderate and lower momenta a reasonable fraction of the pions are produced by reactions off the gluons within the target. Other determinations of Δg have depended upon higher order effects such as the evolution of the polarized quark distributions [19], which is driven in part by Δg .

I will begin by presenting results for $\vec{\gamma} + \vec{n} \rightarrow \pi^\pm + X$ and for $\vec{\gamma} + \vec{p} \rightarrow \pi^\pm + X$ where the photon comes from radiation off an incoming electron beam of energy $E_e = 50\text{GeV}$ and the pions are observed at lab angle $\theta_{lab} = 5.5^\circ$. The outcome plotting asymmetry E vs. the magnitude of the pion momentum is given in Figs. 3.4 and 3.4 using three differing sets of polarized parton models.

The polarized parton models are those of Gehrmann and Stirling (GS) [7], of Glück, Reya, Stratmann, and Vogelsang (GRSV) [8], and a suggestion of Soffer *et al.* [9]. Both the GS and GRSV polarized fits use the fits of Glück, Reya, and Vogt (GRV) [29] when they need unpolarized distributions, at least in leading order. When using the Soffer *et al.* suggestion, it is teamed with the CTEQ [10] quark distributions and the polarized gluon distribution of Brodsky, Burkhardt, and Schmidt (BBS) [20]. In addition this case requires

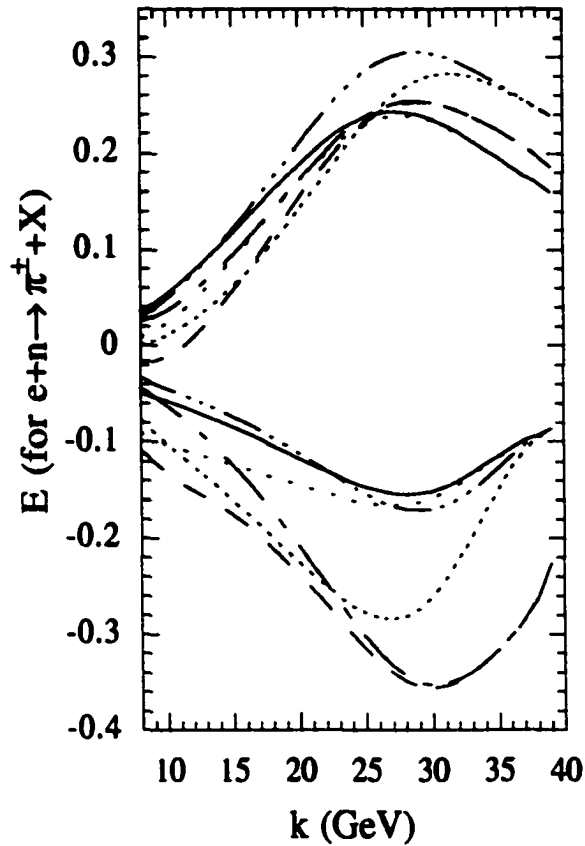


Figure 3.7: The asymmetry E for $\bar{\gamma} + \bar{n} \rightarrow \pi^{\pm} + X$, at $E_e = 50$ GeV and $\theta_{lab} = 5.5^\circ$. The upper six curves are for π^- production and the lower six curves are for π^+ production. For each set of six, there are three curves with the full calculation, with the loose dotted curve using parton distributions from GRSV, the dashed curve using GS-A, and the tight dotted line using CTEQ/Soffer *et al.* and the BBS polarized gluon distribution. The other three curves have Δg set to zero, with the solid line using GRSV, the dash-dot curve using GS, and the dash-triple dot curve using CTEQ/Soffer *et al.*

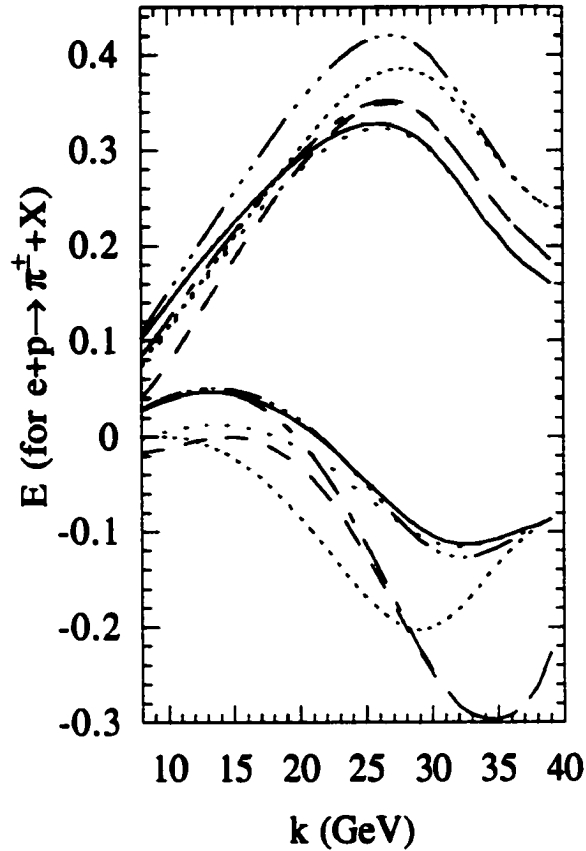


Figure 3.8: The asymmetry E for $\bar{\gamma} + \bar{p} \rightarrow \pi^{\pm} + X$, at $E_e = 50$ GeV and $\theta_{lab} = 5.5^\circ$. This time, the upper six curves are for π^+ production and the lower six curves are for π^- production. As in Fig. 3.4, for each set of six, there are three curves with the full calculation, with the loose dotted curve using parton distributions from GRSV, the dashed curve using GS-A, and the tight dotted line using CTEQ/Soffer *et al.* and the BBS polarized gluon distribution. The other three curves have Δg set to zero, with the solid curve using GRSV, the dash-dot curve using GS, and the dash-triple dot curve using CTEQ/Soffer *et al.*

a polarized distribution for the sea quarks, which is taken as

$$\Delta s(x) = -0.667(1-x)^7, \quad (3.21)$$

with the same sea distribution for up, down, and strange quarks. This gives $\langle \Delta s + \Delta \bar{s} \rangle = -1/6$. In all cases, I set the renormalization scale μ^2 to k_T^2 , where k_T is the transverse momentum of the produced meson.

Although there are 12 different curves on Fig. 3.4, it is not so complicated. In all cases, E is generally positive for the π^- and negative for the π^+ , so there are six curves above for the π^- and six below for the π^+ . Each of the three parton distribution models is represented twice, once with the full calculation and once with the polarized gluon distributions $\Delta g(x)$ (but not the total gluon distribution $g(x)$) set to zero.

Fig. 3.4, for the proton target, is similar except that π^+ is above and π^- below.

One reaches the following conclusions from the graphs:

- At large pion momentum k contributions from gluons in the target are not significant but the results for differing polarized quark distributions are quite different, allowing the data to discriminate among the various polarized quark distribution models. Note that for both the π^\pm at high k , two of the models give quite similar results and one is different. However, for the π^- it is CTEQ/Soffer *et al.* that is different, whereas for the π^+ it is GS that stands out.
- At low or moderate k the results for the different model polarized quark distributions are—if evaluated with zero or the same Δg —rather similar. In the figures, I show the curves with $\Delta g = 0$. The clearest case is π^- production off a proton target.
- At low or moderate k , the differences among the models are mainly due to the differences in Δg (even noting that the largest Δg are not represented on these two figures), and thus the measurements can discriminate among the differing models for Δg .

I elaborate on the last point in Fig. 3.4, where I use only one quark distribution, but six different gluon distributions to show the differences in their effect upon this asymmetry. Two of the new polarized gluon distributions are from Ball, Forte, and Ridolfi (BFR) [19], and I use versions AR and OS. (Neither BBS nor BFR give quark distributions for each individual flavor quark and antiquark, so the results from their gluon distributions can be shown only in combination with other authors's models for the quarks.) The other new polarized gluon distribution is GS version C. One can see that the available polarized gluon distributions, all inferred from g_1 data, sometimes abetted by pQCD considerations at high x [20], give distinct results in the present case.

Incidentally, the minimum x that enters the calculation of the fragmentation process is the same as the unique x that enters the direct process, Eqn. (3.12). Hence for the situation of Figs. 3.4 or 3.4, the minimum x for pion momentum $k = 8$ GeV is $x_{min} = 0.05$ and for $k = 20$ GeV, $x_{min} = 0.16$. This gives some idea of the x range that is probed by these experiments.

I continue showing results in Fig. 3.4 by giving the analog of Fig. 3.4 but for a proton target. The electron energy is still $E_e = 50$ GeV and $\theta_{lab} = 5.5^\circ$. The π^- curves, which are the lower ones in this Figure, bunch very well at low k for the three curves with Δg set to zero, and the curves using the Δg pertinent to each model are quite distinct. The π^+ curves are less distinct from each other, but it is still true that for the models chosen the curves with $\Delta g = 0$ all lie, at low k , above the curves with gluon polarization included.

The next three figures show the analogs of the preceding three Figures but for an incoming electron energy of 27.5 GeV; the lab angle is still $\theta_{lab} = 5.5^\circ$. Fig. 3.4 shows the asymmetry E for π^\pm production off a neutron target for the three models I have chosen, with and without Δg . Fig. 3.5 does the same for a proton target. The Figure with one quark distribution model but six polarized gluon distribution models is Fig 3.5. It is the

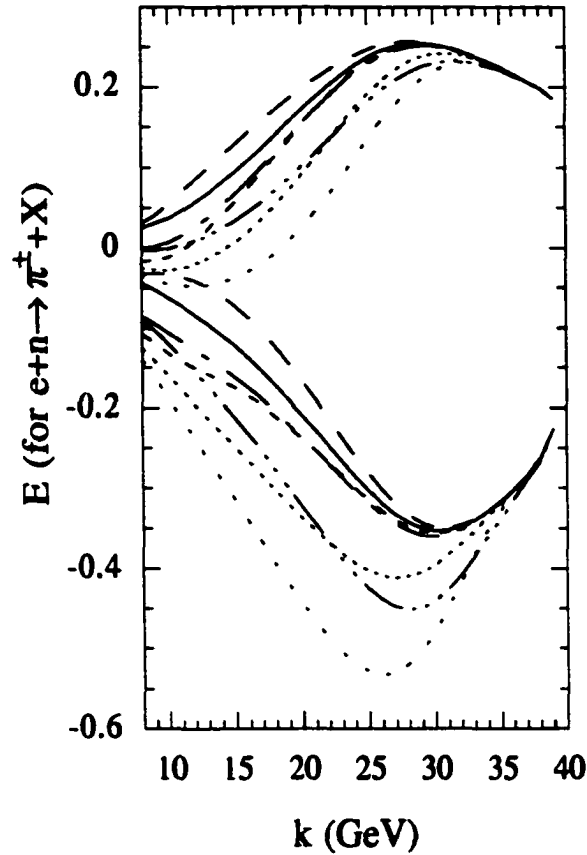


Figure 3.9: The asymmetry E for $\bar{\gamma} + \bar{n} \rightarrow \pi^\pm + X$, at $E_e = 50$ GeV and $\theta_{lab} = 5.5^\circ$, with one model for the quark distributions and several models for the polarized gluon distribution. I choose to use the quark distributions of GS. The solid curve is the benchmark with Δg set to zero. The short dashed curve uses the quark and unpolarized gluon distribution of GS but the polarized gluon distribution of GS model A. The long dashed curve uses GS model C. The dash dot curve uses GRSV. The dash triple dot curve similarly uses BBS, the tight dotted curve uses BFR model AR, and the loose dotted curve uses BFR model OS.

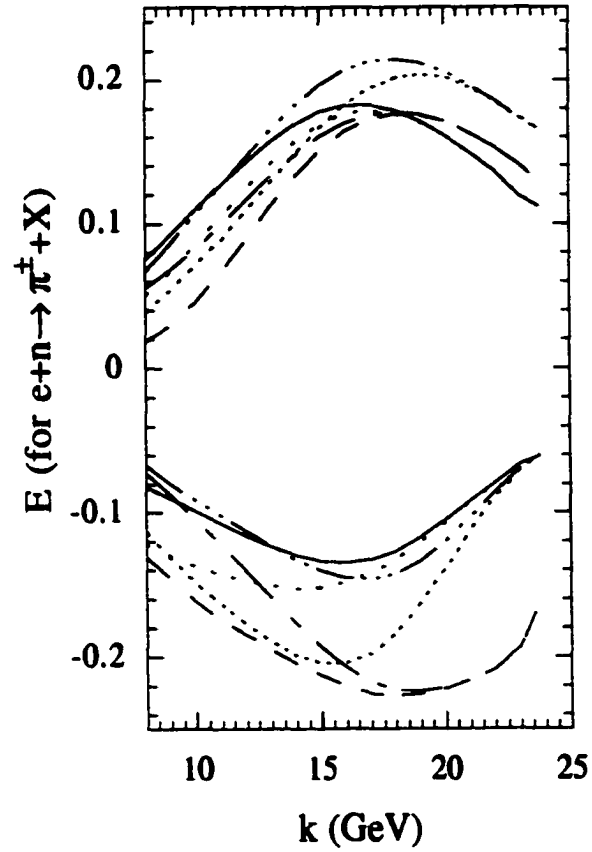


Figure 3.10: The asymmetry E for $\bar{\gamma} + \bar{n} \rightarrow \pi^{\pm} + X$, at $E_e = 27.5$ GeV and $\theta_{lab} = 5.5^\circ$. The remainder of the caption is the same as for Fig. 3.4.

analog of Fig. 3.4 , but for variation this Figure is given with a proton instead of a neutron target.

3.5 Discussion

I feel I have demonstrated that with polarized initial states, pion photoproduction at low (but still with k_T above about 1 GeV) and moderate pion momenta can be a useful and successful way to learn about the polarized gluon distribution. In this region, the various models for the polarized quark distributions all give rather similar results when the effects of the polarized gluon distributions are removed. The effects of the polarized gluon distributions are distinct for the different models, and particularly for the BBS [20] and BFR [19] models are quite large. For the kinematics looked at, the resolved photon contributions are always small. In the low to moderate k region, the fragmentation contribution is dominant.

At the highest allowed pion momentum the asymmetry does become sensitive to the differences among the various quark models, and so can empirically distinguish among them. What I call the direct process, i.e., pion production at short distance rather than via fragmentation, dominates in this region. In particular, the high x quarks of the target give the dominant contributions and the models for the polarized quark distributions do not agree at high x .

Questions may be asked about the use of perturbative QCD, upon which my analyses depend. Since I am mainly considering ratios of cross sections, many of the potential problems will cancel out.

Also, studies of the polarized gluon distribution depend mainly upon the fragmentation process. This is a leading twist process, so using perturbation theory to calculate it should be accurate and has not generally been questioned.

Within the context of perturbation theory, one may ask how large the higher order

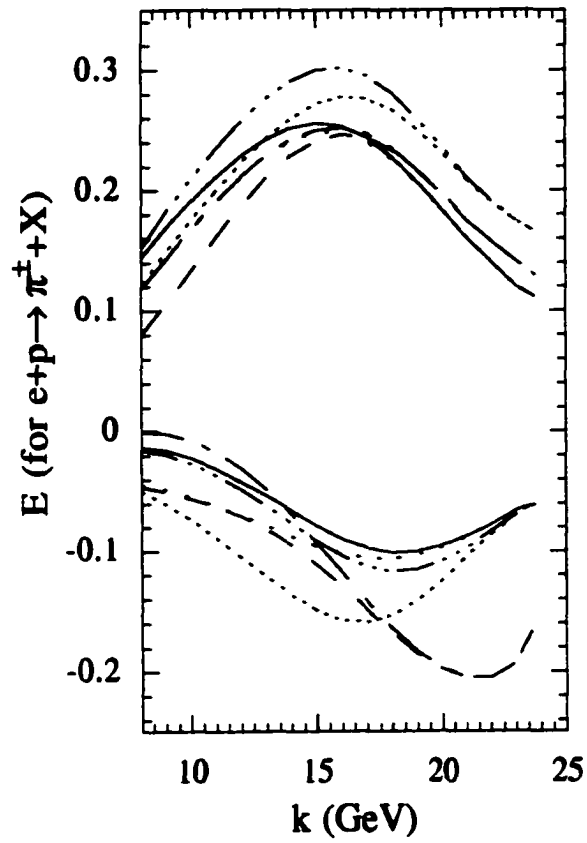


Figure 3.11: The asymmetry E for $\bar{\gamma} + \bar{p} \rightarrow \pi^{\pm} + X$, at $E_e = 27.5$ GeV and $\theta_{lab} = 5.5^{\circ}$. The remainder of the caption is the same as for Fig. 3.4.

in α_s corrections are. For the unpolarized case, the answer is that the next to leading corrections double the result [18]. I should state that I have simply doubled the lowest order calculations to obtain the results: remember we are taking ratios. NLO calculations of $\bar{\gamma}\bar{g} \rightarrow q\bar{q}$ and $\bar{\gamma}\bar{q} \rightarrow qg$ have been done but not were not available at the time of these calculations and were not considered . NLO calculations of $\bar{g}\bar{q} \rightarrow \gamma q$ and $\bar{q}\bar{q} \rightarrow \gamma g$ and related $2 \rightarrow 3$ processes had been done [30]. The K -factors [ratio of LO + NLO to LO cross sections] for the polarized cross section $\Delta\sigma$ always exceed unity, so that the effect of the NLO corrections upon the ratio E for direct photon production is not great.

Much of our further discussion concerns the direct process, which is a higher twist contribution and using perturbative QCD has been questioned in some such cases.

Our analysis requires that the “ X ” in $\gamma + p \rightarrow \pi + X$ is out of the resonance region. For the energies we have considered, this is easy to satisfy except at the highest k .

Another question regards further higher twist corrections, for example, corrections due to the quarks in the pion having finite momentum transverse to the pion’s overall momentum. In the present case, the virtual gluon in the direct process is much farther off shell [4, 17] than for the pion form factor at presently accessible kinematics. Hence higher twist effects will be less significant for measurable photoproduction of high transverse momentum mesons than for meson form factors at any currently measured momentum transfers. Similarly, I have not considered transverse momentum smearing of the incoming quarks. It has been considered in the context of pion production in pp and $\bar{p}p$ collisions, and does have some effect there on the extraction of the polarized gluon distribution [31].

These calculations can also be applied to production of kaons and to neutral pions. For neutral pions, the fragmentation process cross section is the average of the π^+ and π^- cross sections. However, the direct production of neutral pions is less than the direct production of either charged pion. Useful studies are also possible using single polarization

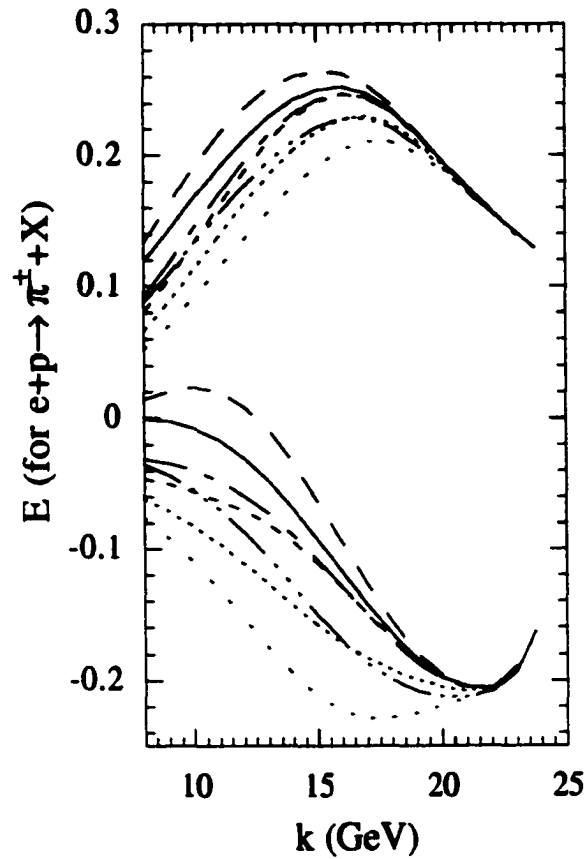


Figure 3.12: The asymmetry E for $\vec{\gamma} + \vec{p} \rightarrow \pi^{\pm} + X$, at $E_e = 27$ GeV and $\theta_{lab} = 5.5^\circ$, with one model for the quark distributions and several models for the polarized gluon distribution. I use the quark distributions of GS. The upper set of curves is for the π^+ and the lower set is for the π^- ; otherwise the caption is the same as Fig 3.4.

asymmetries.

I conclude with a summary.

- Of the three processes that contribute to high k_T pion production, or to its single arm electron equivalent $e + N \rightarrow \pi + X$, the resolved photon process is unimportant for incoming energies of a few 10's of GeV and small angles. The fragmentation process dominates at low or moderate momenta, the direct process dominates at high pion momenta.
- The π^+/π^- ratio predictions are different for fragmentation and direct processes. For isoscalar or near isoscalar targets, with pions at high momenta, fragmentation would give about a 4:1 ratio [coming from $(e_u/e_d)^2$] but the direct process gives about 1:1. Verification that short distance production takes over from fragmentation production lies in seeing a fall in the π^+/π^- ratio (still for $I = 0$ targets) as the takeover occurs.
- Where the direct process dominates, and without polarization, the rate is proportional to things that are known and the I_π , the same integral over the pion distribution amplitude that fixes $\gamma^* + \gamma \rightarrow \pi^0$ and $\gamma^* + \pi^\pm \rightarrow \pi^\pm$. Currently data for the last two processes taken at face value gives discordant values of I_π .
- With initial state polarization, one can form the double helicity asymmetry A_{LL} or E . Where the direct process dominates, at high pion momentum, the asymmetry is proportional to the polarized quark distributions Δu for the π^+ and Δd for the π^- , times things that are known or easily calculable. Hence, one can measure the Δq_i individually.
- When the fragmentation process dominates, experiments with initial state polarization are sensitive to Δg . The polarization asymmetry is 100% in magnitude for the

production off a gluon target, and the current spectrum of models for Δg leads to a wide diversity of A_{LL} or E predictions for pion photoproduction in the fragmentation region.

.

Chapter 4

Soft Contributions to Hard Pion Photoproduction

4.1 Introduction

Recent results [32] on pion photoproduction or, more precisely, low- Q^2 electroproduction, show a need for a careful estimate of soft contributions. In particular, the measured polarization dependent effects are not in good overall agreement with calculations based only on QCD calculated using perturbation theory (pQCD). A key issue is where and if the high transverse momentum cross section is dominated by perturbatively calculable contributions and where soft contributions are important. In the region where perturbative contributions dominate, it is known how hard pion photoproduction can be a source of information about hadron structure as seen in previous chapters.

Pion photoproduction at high transverse momentum, or hard pion photoproduction, supplements what can be learned in the standard hadron structure probes of deep inelastic scattering and Drell-Yan processes, lately joined by high- Q^2 coincident meson pro-

duction [2]. A particular feature of high transverse momentum pion photoproduction with polarized initial states is the sensitivity to the polarized gluon distribution, Δg , in leading order. This contrasts to the other processes mentioned, which have no leading order gluon contribution. Additionally, in some kinematic regions the process occurs mainly due to pion production at short distances (“direct pion production”), whereupon there is sensitivity to the high- x valence quark distribution and the short distance pion wave function.

Many authors have calculated perturbative contributions to hard pion photoproduction, and Chapter 2 centered on short distance pion production, polarization effects were included in Chapter 3, and complete next to leading order corrections have been done [35]. These calculations do include the hard or short distance contributions from hadronic components of the photon, under the heading of resolved photon processes, but do not include the soft part. Here I present a phenomenological calculation of soft contributions, and compare its size to the pQCD results already known. The calculation relies on vector dominance (VMD), which is a way to represent the hadronic components of the photon as they enter into soft processes. Experimental studies, in particular the Omega [36], H1 [37], and Zeus [38] collaborations, have shown that hadron induced and photon induced hadron production were proportional to each other up to a certain transverse momentum, and that above this transverse momentum the photon induced reactions rise relative to hadron induced ones as the pointlike piece of the photon becomes more important. For the kinematics of the above experiments it is about 2 GeV transverse momentum where the pointlike photon begins to become apparent.

The next section, puts together known photon vector meson couplings with phenomenological representations of the hadron-hadron reactions to produce soft cross section formal results for kinematics of interest. Following that, section 4.3 presents some numerical results for cross sections and polarization effects, making an assumption that the polariza-

tion dependence of the soft processes is small. I close with a discussion in section 4.4.

4.2 Outline of Calculations

There are quite successful descriptions of soft processes that have been obtained using Regge theory inspired models [39]. However, the sophistication of these models makes them somewhat rich in parameters that need to be set from the same data that is being described, or from similar data. For example, there is a need for some cutoffs whose scale parameters are not predicted from theory, a use of different Pomeron intercepts for single diffractive processes and total cross sections, and a fitting of the overall size in the form of the triple Pomeron coupling using related reactions. I opt for a complementary course, wherein one simply uses known couplings to calculate photon to vector meson conversion and then use measured data for the hadronic cross sections.

For definiteness I will consider π^+ production off a proton target.

The ρ -dominance amplitude is

$$f(\gamma p \rightarrow \pi^+ X)|_{\rho} = \frac{e}{f_{\rho}} f(\rho^0 p \rightarrow \pi^+ X) \quad (4.1)$$

and

$$\begin{aligned} d\sigma(\gamma p \rightarrow \pi^+ X) &= \frac{\alpha}{\alpha_{\rho}} d\sigma(\rho^0 p \rightarrow \pi^+ X) \\ &+ \text{other VMD} + \text{non VMD contributions,} \end{aligned} \quad (4.2)$$

where $\alpha_{\rho} \equiv f_{\rho}^2/4\pi$ and 'other VMD' stands for contributions of excited ρ 's and of other vector mesons. The value of α_{ρ} can be obtained from $\Gamma(\rho \rightarrow e^+e^-)$ and is [40]

$$\alpha_{\rho} = 2.01 \pm 0.10. \quad (4.3)$$

This reduces the problem to finding the cross section or a parameterization thereof for vector meson production of the π^+ . In principle, this might be an experimentally measurable process, but in practice we will have to approximate it by charged pion induced processes. The remainder of this section is mostly devoted to explaining how to do this. First I make some remarks on contributions from excited ρ 's and other vector mesons.

Excited ρ contributions to $\gamma p \rightarrow \rho + X$ decrease the rate by 20%, according to Pautz and Shaw [40]. The basic relation is

$$f(\gamma p \rightarrow \rho X) = \frac{e}{f_\rho} \underbrace{f(\rho p \rightarrow \rho X)}_{\text{"}f_{\rho\rho}\text{"}} + \frac{e}{f_{\rho'}} \underbrace{f(\rho' p \rightarrow \rho X)}_{\text{"}f_{\rho'\rho}\text{"}} \quad (4.4)$$

and the claim is that while the couplings are about the same, the amplitudes interfere destructively,

$$f_{\rho'\rho} \approx (-16\%) f_{\rho\rho}. \quad (4.5)$$

The effect can be subsumed by simply calculating simple vector meson dominance with $\alpha_\rho^{eff} = 2.44$. The question is whether the same is true for π^+ production,

$$f_{\rho'\pi} \stackrel{?}{\approx} (-16\%) f_{\rho\pi}, \quad (4.6)$$

and I shall proceed assuming it is true.

From flavor SU(3), the couplings of the photon to the vector mesons lie in the ratios

$$f_\rho^{-2} : f_\omega^{-2} : f_\phi^{-2} = 9 : 1 : 2. \quad (4.7)$$

If the ρ , ω , and ϕ strong interaction cross sections are the same, then the other flavors add 33% to the ρ contribution. At the present level of knowledge, it is appropriate to approximate the total VMD contribution by the ρ contribution multiplied by 4/3. The photoproduction cross section is now

$$d\sigma(\gamma p \rightarrow \pi^+ X) = \frac{4}{3} \frac{\alpha}{\alpha_\rho^{eff}} d\sigma(\rho^0 p \rightarrow \pi^+ X) + \text{non VMD contributions}, \quad (4.8)$$

with $\alpha_\rho^{eff} = 2.44$. Off shell effects have not been considered.

A representation, of $d\sigma(\rho^0 p \rightarrow \pi^+ X)$ is needed. Often used is,

$$d\sigma(\rho^0 p \rightarrow \pi^+ X) = \frac{1}{2} d\sigma(\pi^+ p \rightarrow \pi^+ X) + \frac{1}{2} d\sigma(\pi^- p \rightarrow \pi^+ X). \quad (4.9)$$

This will not work in the forward direction, where one cross section has a leading particle effect but $\rho^0 p \rightarrow \pi^+ X$ should not. One may expect the measurable cross section most similar to $\rho^0 p \rightarrow \pi^+ X$ would be $\pi^+ p \rightarrow \pi^0 X$. Data from O'Neill *et al.* [41] show that $\pi^+ p \rightarrow \pi^0 X$ has the same angular dependence as $\pi^+ p \rightarrow \pi^- X$ but is about 30% larger. This reduces the problem to finding a representation of the latter.

Bosetti *et al.* [42], who experimentally studied charged pion cross sections, found that the cross section $\pi^+ p \rightarrow \pi^- X$ factors in k_T and ξ , where ξ is the scaled rapidity,

$$\xi = \frac{y - y_t}{y_p - y_t} \quad (4.10)$$

for $p =$ projectile and $t =$ target, and y is the rapidity, which may be defined in various equivalent ways including

$$y = \text{arcsinh} \frac{p_L}{\sqrt{p_T^2 + m^2}}. \quad (4.11)$$

That means,

$$\omega_\pi \frac{d\sigma}{d^3k} = \omega_\pi \left. \frac{d\sigma}{d^3k} \right|_{90^\circ \text{CM}} \times g(\xi), \quad (4.12)$$

where $g(\xi)$ will have some dependence on k_T to respect kinematic bounds. A choice that appears to work is

$$g(\xi) = \left(1 - \frac{(\xi - \xi_0)^2}{(\xi_{max} - \xi_0)^2} \right)^2, \quad (4.13)$$

where ξ_0 is halfway between ξ_{max} and ξ_{min} , and $\xi_{max,min}$ are the maximum or minimum ξ for a given k_T .

Beier *et al.* [43] have analytic forms that work over a wide kinematic range for $pp \rightarrow \pi^- X$ at 90° in the CM, and the Bosetti *et al.* data [42] approximately agree with

$$\omega_\pi \frac{d\sigma}{d^3k}(\pi^+ p \rightarrow \pi^- X) = \frac{2}{3} \omega_\pi \frac{d\sigma}{d^3k}(pp \rightarrow \pi^- X). \quad (4.14)$$

In summary, calculate using

$$\begin{aligned} \omega_\pi \frac{d\sigma}{d^3k}(\gamma p \rightarrow \pi^+ X) = & \\ + \frac{\alpha}{\alpha_\rho^{eff}} \cdot 1.3 \cdot \frac{4}{3} \cdot \frac{2}{3} \cdot \omega_\pi \frac{d\sigma}{d^3k}(pp \rightarrow \pi^- X) \Big|_{90^\circ \text{CM}} & g(\xi) \\ + \text{non VMD contributions.} & \quad (4.15) \end{aligned}$$

The “non VMD” contributions are discussed in, for example, [33–35]. To review the numerical factors, the single charge change reaction was about 1.3 times the double charge change reaction according to [41], the $4/3$ is to account for the ω and ϕ mesons, and the $2/3$ is so that one may use pp cross section parameterizations as stand-ins for meson-proton cross sections. Electroproduction data with particle identification with electron energies up to 19 GeV, reported in Wisner's thesis [44], indicate that π^- production off a proton target is about a factor 1.3 lower than for the π^+ , and that π^\pm is produced off a neutron at about the same rate as π^\mp off a proton.

The connection between photoproduction and electroproduction when the outgoing electron is unobserved is given by the Weizäcker-Williams equivalent photon approximation,

$$d\sigma(eN \rightarrow \pi X) = \int_{E_{min}}^{E_e} dE_\gamma N(E_\gamma) d\sigma(\gamma N \rightarrow \pi X). \quad (4.16)$$

The expressions used for the photon number density $N(E_\gamma)$ and the lower limit are quoted in [34].

4.3 Some Results

I begin by examining the differential cross section for one relevant kinematic situation, namely that with 50 GeV incoming electrons with pions emerging at 5.5° in the lab. This energy is typical of SLAC and not far above what can be obtained at HERMES. Fig. 4.3 shows the unpolarized differential cross section vs. pion momentum for both the π^- and π^+ . There are three curves on each plot, the soft contribution represented by VMD and two perturbative contributions, namely parton production followed by fragmentation and direct or short range pion production. (Another perturbative contribution, the resolved photon process is small enough at this energy and angle not to be an issue.) The three contributions should be added incoherently.

The soft contribution continues to a momentum that is higher than expected. Nonetheless, one sees that at momenta beyond about 25 GeV for the π^- or 22 GeV for the π^+ , the sum of the perturbative contributions exceed the soft contributions. For this angle, this is about 2.4 and 2.1 GeV of transverse momentum, respectively.

The hadron to electron ratio is also measured and reported in the experimental paper [32]. At lower momenta the calculated π/e ratio is too small without the VMD contributions. With all contributions added together, the calculated pion to electron ratio is shown in Fig. 4.3. These are in reasonable accord with the plots presented in [32], which in turn are stated to be in reasonable accord with the data.

Having a reasonable description of the unpolarized cross section in hand, one needs to consider the polarization asymmetry. If R and L represent photon helicities and \pm represent target helicities, then the longitudinal asymmetry E or A_{LL} is defined by

$$E = A_{LL} \equiv \frac{\sigma_{R+} - \sigma_{R-}}{\sigma_{R+} + \sigma_{R-}}. \quad (4.17)$$

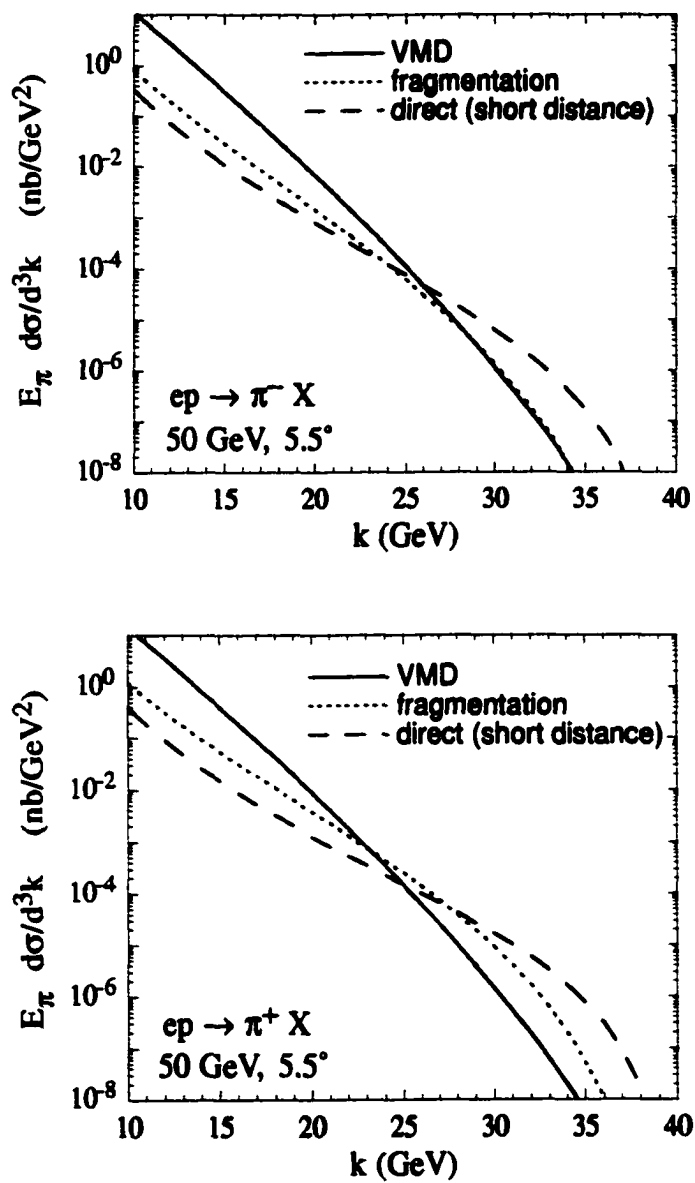


Figure 4.1: The invariant differential cross sections for $ep \rightarrow \pi^- X$, above, and π^+ , below. The incoming electron energy is 50 GeV, and pion lab angle is 5.5°.

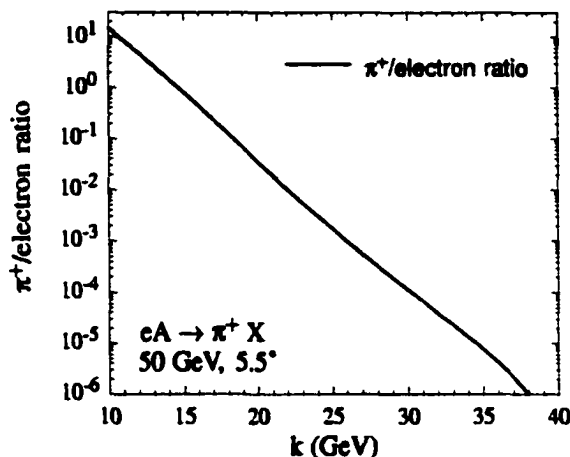


Figure 4.2: The calculated pion to electron ratio for a $^{15}\text{N He}_3$ target. For this target and this vertical scale, the π^- results are hardly distinct from the π^+ . They are in reasonable accord with data as reported in [32].

The polarization dependence of the perturbative terms is calculable, but there is no direct polarization information on the VMD contributions. One class of VMD subprocess would give a negative polarization asymmetry if hadron helicity conservation holds for those diagrams. This is the reaction $V + q \rightarrow \pi + q$, where V stands a vector meson which must have helicity ± 1 since it comes from conversion of a real photon. The the vector meson and initial quark must have opposite helicity, or else the final state must have total helicity $\pm 1/2$. However, Manayenkov [45] has argued from a Regge analysis that the soft contributions to A_{LL} are small. Here, I shall assume no polarization dependence for the VMD terms. The polarization asymmetry then comes only from the perturbative terms, but it is much muted at low momentum because of the large non-perturbative cross section.

Actual polarization asymmetry results plotted vs. pion momentum, again for electron energy 50 GeV and pion angle 5.5° , are shown for proton targets in Fig. 4.3 and for deuteron targets in Fig. 4.3. (The deuteron in this calculation is treated simply as a proton

plus a neutron.) Also shown are polarization asymmetry data [32] for charged hadrons and for identified π^\pm .

A few words should be said about the distribution functions and fragmentation functions. GRSV [8] and GS [7] are both widely used, and BBS [20] differ from them most notably in having the pQCD counting rule results for the d-quark to u-quark ratio for large x , and by not nicely separating sea quark contributions. Since the distribution functions are most needed at large x , the latter may not be so serious. The d/u ratio now appears, with more careful examination of how the neutron structure functions are extracted from deuteron data [46], to the pQCD ratio of 1/5 rather than to zero, which makes it important to notice how different the BBS results are from the others at high momenta.

I used the fragmentation functions given in equation (A.1 and A.2) and experience has shown that the results at least at SLAC or HERMES energies would not be too different for the π^+ but larger in magnitude for the π^- if I used those of Binneweis et al [27]. For the BBS distribution, I present results from one additional fragmentation function given in equation (A.5).

4.4 Discussion

I believe I have presented as accurate an estimate of the soft processes in pion photoproduction as can currently be done. Improvements could follow given more information. For examples, the connections made in section 4.2 require some leaping among processes, and I have not included pions from target fracture in the perturbative cases, nor have I deeply entered into the questions newly revived about the unfavored fragmentation functions. I feel the latter is an important question that should be the subject of a separate study. Having made these caveats, I have a clear and logical representation of the soft contributions that I can compare to the newest pion photoproduction (or low Q^2 electro-

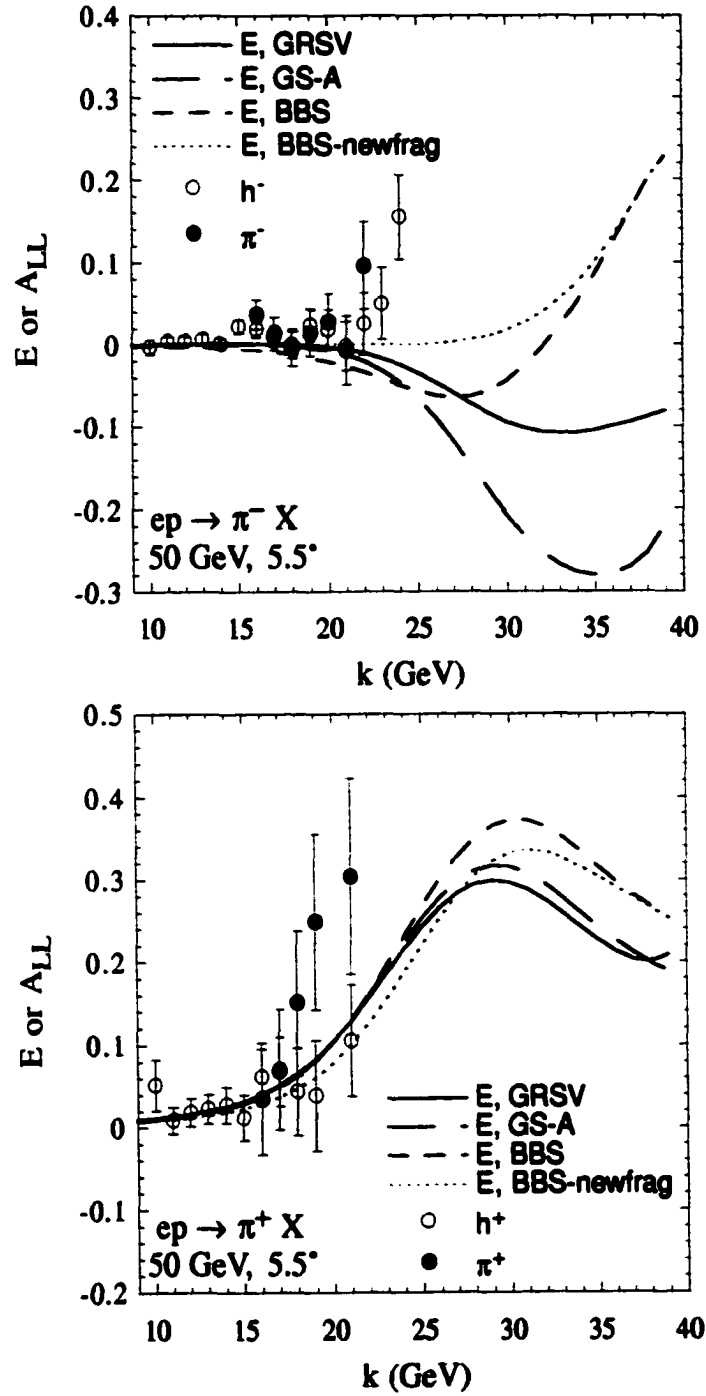


Figure 4.3: Polarization asymmetries for $ep \rightarrow \pi^-$, above and π^+ , below. The data for charged hadrons and for charged pions is from [32].

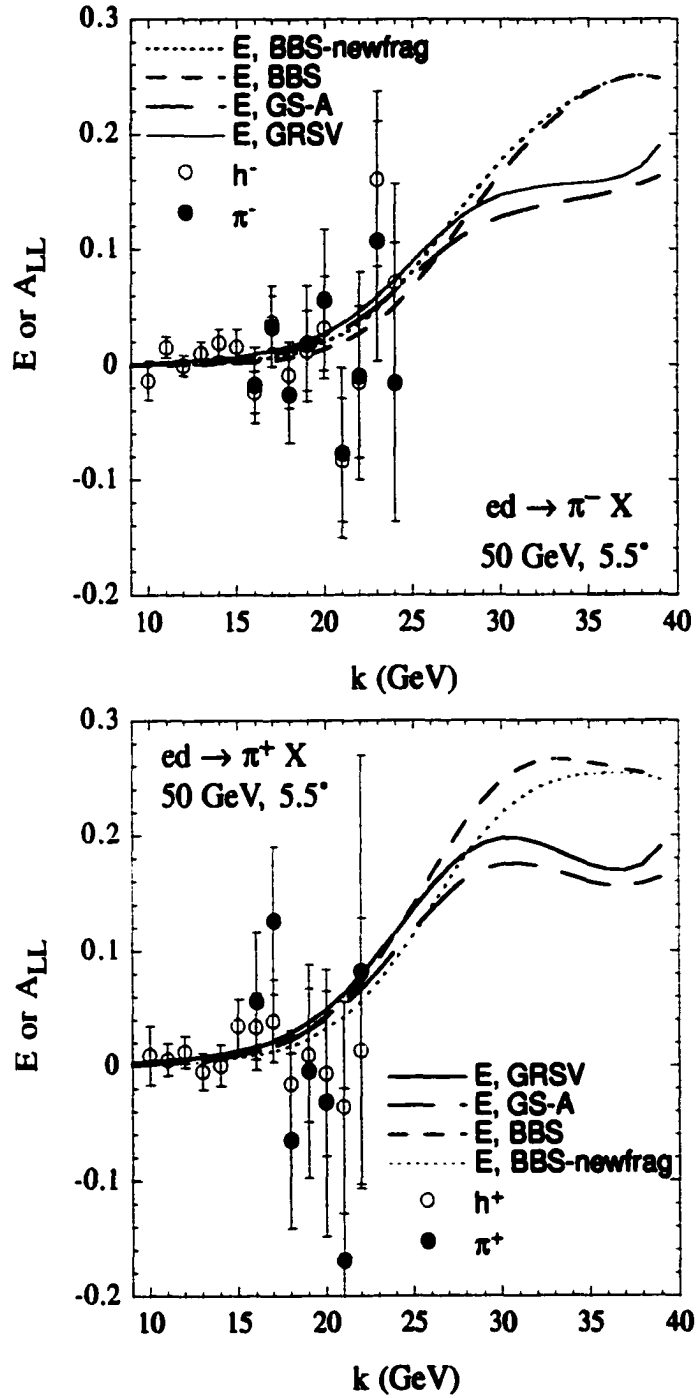


Figure 4.4: Polarization asymmetries for the deuteron, with $ed \rightarrow \pi^- X$ above and $ed \rightarrow \pi^+ X$ below. The data is from [32].

production) data. I find that the soft process, working through VMD, can explain the total cross section at lower transverse momentum.

I find further that the data is compatible with the idea that there is little polarization asymmetry in the soft interactions, as may be seen in comparisons to the data in Figs. 4.3 and 4.3. One would like to be able to confirm or understand this by other means.

Perturbation theory can be used to calculate the cross section and polarization dependence at higher transverse momentum. The crossover is at a bit over 2 GeV for the kinematic regions dealt with here. The idea that hard pion photoproduction is sensitive to Δg is true in a region where pQCD is valid and the fragmentation process dominates. As a reminder, it is true because the gamma-gluon fusion process accounts for a reasonable fraction of the hard pion photoproduction, and this process has a magnitude 100% polarization asymmetry. However, it requires somewhat more energy so that there is a region above the VMD region where the fragmentation process is important. As an example, I present in Fig. 4.4 a differential cross section for 340 GeV electrons impinging on an standing proton with pions emerging at 1.34° . (This corresponds to a collider with 4 GeV electrons hitting 40 GeV protons and pions emerging at 90° in the lab. The energies are pertinent to an Electron Polarized Ion Collider under discussion at the Indiana University Cyclotron Facility.) The sort of region wanted is seen between about 2 and 6 GeV of transverse momentum.

I have been greatly motivated by the idea that hard pion photoproduction can give information on parton distributions. This is already proving feasible. The H1 collaboration, working in a region where the resolved photon process dominates, has extracted the gluon density in the photon from data on this process [48].

The idea that the ratio $d(x)/u(x)$ obeys the pQCD limit for large x , rather than falling to zero, is gaining ground. So far the relevant analyses [46] are only for the unpolarized case, but the $x \rightarrow 1$ polarization prediction of 100% polarization parallel to the parent

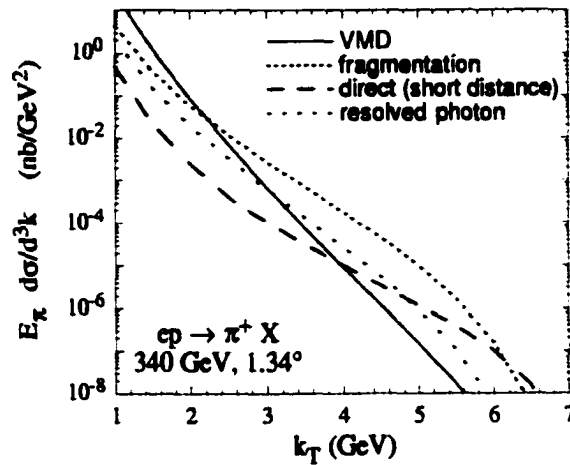


Figure 4.5: The differential cross section for 340 GeV electrons impinging on an standing proton with positive pions emerging at 1.34° . (This corresponds to a collider with 4 GeV electrons hitting 40 GeV protons and pions emerging at 90° in the lab.)

hadron can be tested here. With direct pion production (or also with fragmentation) off valence quarks dominant at the highest E_π , one has an asymmetry for the π^- of

$$E = A_{LL} = \frac{s^2 - u^2}{s^2 + u^2} \cdot \frac{\Delta d}{d} = 0.24 \frac{\Delta d}{d} \quad (4.18)$$

where the number is for $E_e = 50$ GeV, pion $\theta_{lab} = 5.5^\circ$, and the highest allowed E_π (in this case, 41.2 GeV). For pQCD as $x \rightarrow 1$ one has $\Delta d = d$, and one can see this trend in the results for the BBS [20] distribution functions since BBS follows the pQCD limit. In fact, for pQCD the limiting asymmetry is the same for π^\pm and independent of target.

Chapter 5

Scaling and Duality in Semi-exclusive Processes

5.1 Introduction

Scaling is a well-established phenomenon in deep inelastic scattering (DIS). The cross section with specific kinematic factors removed gives structure functions that depend on only the scaling variable x_B , up to calculable logarithmic corrections. In addition, an inclusive-exclusive connection—“Bloom-Gilman scaling” [49]—is observed in these totally inclusive (at least on the hadronic side) reactions. Duality in this situation means that resonance bumps observed in the structure functions at low momentum transfers Q^2 average out to the smooth structure function measured at higher momentum transfers but the same x_B . Usually, but not always, duality is realized in such a way that as the resonance peak moves in x_B with changing Q^2 , the ratio of the peak height to the height of the scaling curve evolved from higher Q^2 is constant.

Both scaling and scaling violation have played a crucial role in understanding the

constituents of elementary particles and in establishing QCD as the accepted theory of the strong interactions. Duality is in detail less well understood [50,51]. It seems, however, to show that the fundamental single quark QCD process is still decisive in setting the scale of the reaction in the resonance region, and that the crucial role of the final state interactions in forming the resonance becomes moot when averaged over, say, the resonance width. This last observation, if reliably understood, could allow one to use duality to study the structure functions in the interesting and still experimentally uncertain $x_B \rightarrow 1$ region. For a fixed available energy, $x_B \rightarrow 1$ means getting into the resonance region and if one were sure of the connection of the resonance region average to the scaling curve, one could determine the scaling curve significantly closer to the kinematic upper endpoint.

Departing from DIS, one wants to continue to test one's ability to understand and apply QCD to describe hadronic processes. A set of processes that can be a new testing ground for both scaling and duality phenomena are semi-exclusive reactions typified by

$$\gamma + p \rightarrow \pi + X, \quad (5.1)$$

where the photon may be real or virtual. These processes are the topic of this paper. I shall study suitable kinematic variables for the general case and, when I get more detailed, give special attention to photoproduction with large photon to pion momentum transfer, t .

A first requirement is to find a scaling region. This problem has been studied in the high Q^2 -low (t/Q^2) limit, focusing on the totally exclusive reaction but with extension to the semi-exclusive case [52]. These authors found that scaling functions would exist, provided the photon and pion currents directly and successively interacted with the same quark while the rest acted as spectators.

Here I, concentrating on photoproduction at high $|t|$, show that perturbative QCD (pQCD) predicts there is indeed a scaling region. I shall below show the kinematic factors that connect the cross section to the expected scaling function. I shall also see that the

scaling region does require kinematics where photopion production is dominated by direct interactions of both the photon and the pion [4,34,53], such as seen in Fig. 5.1. In particular, one must avoid regions where the pion comes from soft processes or comes as part of a jet from a fragmenting parton. In earlier work Afanasev et al [33]. were able to show that regions of direct pion production exist, and therefore there are regions where one can find a scaling function.

When scaling is established at high $|t|$, one can study duality. One can ask whether the scaling curve from high Q^2 or t a decent average over the resonance bumps seen at the same x but lower Q^2 or t ? Duality in this sense appears to be true for all the resonances seen in DIS. Further, one can ask if the bump to continuum ratio is constant as Q^2 or t changes? This constancy is seen in DIS for most resonances, but not for the $\Delta(1232)$. While studying the kinematics and working in photoproduction context, one can see that it is possible in a single experiment with good kinematic coverage to probe a given x region over a wide range of m_X from the resonance region to well into the continuum region.

This chapter proceeds as follows. Section 5.2 will discuss the kinematics and scaling variable for the semiexclusive process. Section 5.3 will show how a scaling function emerges for semi-exclusive hard pion photoproduction, and also show the existence of a region where direct pion production dominates, specifically for a situation of 30 GeV incoming photons. Section 5.4 will show that pQCD expectations for the resonance peak/scaling curve ratio at changing $|t|$ are similar to what one sees in DIS. Section 5.5 will offer some conclusions.

5.2 kinematic variables

For the process $\gamma + p \rightarrow \pi + X$, define the Mandelstam variables by

$$s = (p + q)^2, \quad t = (q - k)^2, \quad u = (p - k)^2. \quad (5.2)$$

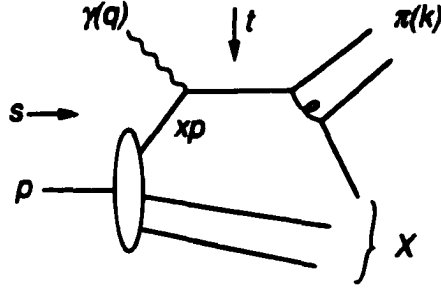


Figure 5.1: Direct (also isolated or short-distance) pion production, with some kinematics indicated.

Define x in general by,

$$x = \frac{-t}{s + u - 2m_N^2 - q^2 - m_\pi^2}, \quad (5.3)$$

and note that all quantities defining x are experimentally measurable [4, 34, 53]. One can show $0 \leq x \leq 1$, and $x = 1$ corresponds to the case that X is a nucleon. Also generally, the hadronic mass recoiling against the pion is given by

$$m_X^2 = m_N^2 - t \left(\frac{1}{x} - 1 \right). \quad (5.4)$$

Specializing to the case where direct pion production, Fig. 5.1, is the underlying process, in the limit of high t or s and high recoil mass m_X , one can show that this x is the fraction of the target's momentum carried by the struck quark. The proof involves defining Mandelstam variables for the subprocess $\gamma + q \rightarrow \pi + q'$. I anticipate the result by letting the momentum of the struck quark be called xp , and get

$$\begin{aligned} \hat{s} &= (xp + q)^2 = x(s - q^2) + q^2, \\ \hat{t} &= (q - k)^2 = t, \\ \hat{u} &= (xp - k)^2 = xu, \end{aligned} \quad (5.5)$$

where I have neglected masses but not q^2 . For the direct pion production subprocess,

$$\hat{s} + \hat{t} + \hat{u} = q^2, \quad (5.6)$$

and substituting Eqn. (5.5) leads to the identification of x the momentum fraction to x the experimental observable, when individual particle masses can be neglected.

Thus x is a precise analog of the observable $x_B = Q^2/2m_N\nu$ in deep inelastic scattering. These formulas should and do connect to the well known ones for deep inelastic kinematics in the limit $k \rightarrow 0$. In this limit, $u \rightarrow m_N^2$ and $t \rightarrow q^2 \equiv -Q^2$ and

$$\begin{aligned} m_X^2 &= m_N^2 + Q^2 \left(\frac{1}{x} - 1 \right), \\ x &= \frac{-t}{s - m_N^2 - q^2} = \frac{Q^2}{2p \cdot q}, \end{aligned} \quad (5.7)$$

without approximation.

Still regarding deep inelastic scattering, Bloom and Gilman [49] found that near threshold scaling worked better if one used a revised variable defined as $1/x'_B = 1/x_B + m_N^2/Q^2$. By analogy to Bloom and Gilman's proposal I could define a modified scaling variable with $-t$ replacing Q^2 :

$$\frac{1}{x'} = \frac{1}{x} + \frac{m_N^2}{-t}, \quad (5.8)$$

whence

$$m_X^2 = -t \frac{1 - x'}{x'}. \quad (5.9)$$

One should keep this possibility in mind here also.

Another situation, related to the one pursued here, is semi-exclusive deep inelastic scattering with parallel kinematics. This means high Q^2 and an observed meson with three-momentum parallel to the incoming photon, in the lab. In this case, there is a variable z defined by

$$z \equiv \frac{p \cdot k}{p \cdot q}. \quad (5.10)$$

and obtain

$$\begin{aligned} m_X^2 &= m_N^2 + Q^2(1-z) \left(\frac{1}{x} - 1 \right), \\ x &= \frac{Q^2}{2p \cdot q}, \end{aligned} \tag{5.11}$$

with the neglect of terms of $\mathcal{O}(m_N^2 x^2 / Q^2)$.

5.3 scaling and kinematic regions

Now I shall focus on hard pion photoproduction, where $q^2 = 0$, k_T is large, and $|t|$ is large.

I will be mainly interested in direct pion production with m_X large, and in the transition to the exclusive reactions $\gamma + N \rightarrow \pi X$. Other processes do contribute. In particular there are soft processes, and processes where the pion is produced as part of the fragmentation of a quark or gluon into a jet. These processes can be evaded if one can go to sufficient transverse momentum. I will comment on them briefly before proceeding.

Soft processes are frequently approximated using vector meson dominance of the photon interaction, illustrated in Fig. 5.3. They are important at low transverse momenta, although the boundary between “low” and “high” is higher than one might expect, namely around 2 GeV. Afanasev et al. have considered these processes in a fashion suitable for the present context in [54]; one can also find a representation of them in PYTHIA [39].

Moderate transverse momenta hard pions can be produced by a fragmentation of a parton. The process is perturbatively calculable and could be a way to learn about polarized or unpolarized gluon distributions of the target [34,35]; one example is illustrated in Fig. 5.3.

Neither the fragmentation nor the soft process is useful for the present duality study. The reason is that the experimental x variable for them does not have a unique connection to the quark momentum fraction, and I will not be able to prove a scaling relation for them.

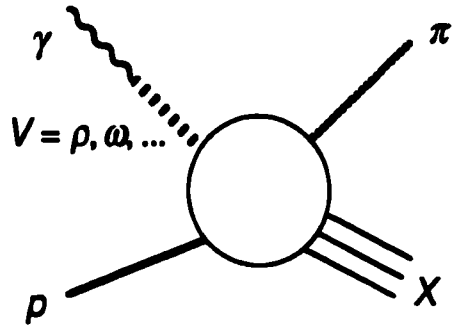


Figure 5.2: Soft processes, approximated by vector meson dominance.

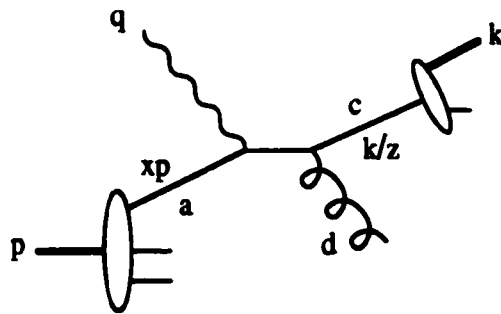


Figure 5.3: A fragmentation process, with the pion's momentum labeled as k .

Direct pion production, however, does have the nice connection between an experimentally observable x and the struck quark momentum fraction, and it is calculable in pQCD. It is a higher twist process. Factors of the decay constant enter the amplitude, representing the quark-antiquark wave function of the pion at the origin, and must be dimensionally compensated by an extra power of s in the cross section. Nonetheless, direct pion production can dominate over fragmentation at high k_T because it always gives all the transverse momentum in the pion direction to the one pion. In the fragmentation process the observed pion has a share of a jet momentum determined by a fragmentation function, and for high k_T , when the pion must take most of the momentum of the jet, the fragmentation function becomes small.

For the direct process, an operational scaling function $F(x, s, t)$ can be defined by

$$\begin{aligned} E_\pi \frac{d\sigma}{d^3k} &= \frac{(s - m_N^2)x^2}{-\pi t} \frac{d\sigma}{dx dt} \\ &= \frac{(s - m_N^2)x^2}{-\pi t} \frac{d\hat{\sigma}}{dt}(\gamma q \rightarrow \pi q') F(x, s, t). \end{aligned} \quad (5.12)$$

I.e., the scaling function is related to the cross section by some kinematic factors. One set of factors is explicit above, and the other is always taken to be the perturbative cross section for the subprocess, which is [4, 34]

$$\begin{aligned} \frac{d\hat{\sigma}(\gamma q \rightarrow M q')}{dt} &= \frac{128g_F^2\pi^2\alpha_s^2}{27(-t)\hat{s}^2} I_M^2 \left(\frac{e_q}{\hat{s}} + \frac{e_{q'}}{\hat{u}} \right)^2 \\ &\times [\hat{s}^2 + \hat{u}^2 + \lambda h (\hat{s}^2 - \hat{u}^2)], \end{aligned} \quad (5.13)$$

where one should substitute quark charges relevant for pion being produced, for example $e_q = e_u$ and $e_{q'} = e_d$ for the π^+ . The flavor factor g_F is unity for the π^\pm and $1/\sqrt{2}$ for the π^0 . I_M is given in terms of the distribution amplitude of the meson as $\int d\xi_1 \phi_M(\xi, \mu^2)/\xi_1$. For the asymptotic distribution amplitude, $I_\pi = \sqrt{3}f_\pi/2$ with $f_\pi \approx 93$ MeV.

Polarization dependence has been included for future use: λ is the helicity of the

photon and h is twice the helicity of the target quark. Of course, duality can be tested with polarization as well as without.

The reason to believe that the above expression, Eqn. (5.12), produces a scaling formula is that the perturbative formula valid for short distance pion production (the process of Fig. 5.1) is,

$$E_\pi \frac{d\sigma}{d^3k} = \frac{(s - m_N^2)x^2}{-\pi t} \times \sum_q \frac{d\hat{\sigma}}{dt}(\gamma q \rightarrow \pi q') G_{q/T}(x, \mu^2) \quad (5.14)$$

Thus where perturbation theory works, there is a scaling function $F(x, s, t)$ is mainly dependent on x . One can relate it to the quark distributions (with weak dependence on the scale μ^2 , which we may set to t), as in DIS. One expects the formulas will be mainly applied in the high x region, where valence quarks dominate.

A comment on the fact that the presence of a hard gluon exchange (see Fig. 5.1) indicates that one needs sufficiently high energies to apply the pQCD formalism. However, since only one pion distribution amplitude is involved for the direct process, if the photon attaches to the produced $q\bar{q}$ pair of Fig. 5.1 (the worse case), the average virtuality of the gluon in question corresponds to the one determining the pion electromagnetic form factor at $Q^2 \approx 20(35) \text{ GeV}^2$ scale, for the asymptotic (Chernyak-Zhitnitsky) pion distribution amplitude assuming a CEBAF energy of 12 GeV, pion emission angle of 22° , and $m_\pi = 2 \text{ GeV}$ (see Ref. [34] for details). Therefore one may hope to observe a single-gluon exchange, which is a higher twist effect, in inclusive photoproduction of pions even at CEBAF energies generally considered not high enough to reach the perturbative QCD domain. Indications of direct pion production off a quark were obtained in πN scattering (see Ref. [55] for references and discussion).

One may now ask if this scaling function dual, in a Bloom-Gilman like sense, to the

bumpier curve one will get in the resonance region? The resonance region, of course, is what exists at the very highest transverse momentum for a fixed s , where there is very little energy left over to put into recoil mass.

Formally, the duality relation then may be written as an integral at fixed t and s of the differential cross section $d\sigma/dx dt(\gamma N \rightarrow \pi X)$, and in the region of the direct process dominance reads

$$\int_{(1-\frac{m_X^2-m_N^2}{s})^{-1}}^1 dx \sum_q G_{q/N}(x) \frac{d\sigma}{dt}(\gamma q \rightarrow \pi q') \propto \sum_R \frac{d\sigma}{dt}(\gamma + N \rightarrow \pi + R). \quad (5.15)$$

Summation in the right hand side of Eqn. (5.15) is done over all resonances R with masses $m_R \leq m_X$, with the nucleon final state included. If the parton distribution function of the nucleon is $G_{q/N} \sim (1-x)^3$ at $x \rightarrow 1$ and the subprocess $\gamma q \rightarrow \pi q'$ cross section is determined by the one-gluon exchange mechanism of Fig. 5.1, then as will be shown in the next section duality as in Eqn. (5.15) requires that the resonance excitation cross section $d\sigma/dt(\gamma + N \rightarrow \pi + R) \propto 1/s^7$ at fixed t/s —the result known from the constituent counting rules [56]. The duality relation above could also be written using the modified scaling variable x' from Eqn. (5.8).

One should ask if the proper regions exist. There needs to be a region where direct pion production dominates, where one can measure the scaling curve and see how it tails off into the resonance region. Such a region does exist. From earlier studies [34, 54] the machinery exists to calculate the direct pion and fragmentation process, and estimate the VMD processes. The direct process has been shown that, even though it is higher twist, does take over at some point if there is enough initial photon energy.

A useful presentation of the calculated results is shown in Fig. 5.3. The figure attempts to show that one can follow a given x region from the resonance region until

well into the scaling region, and do so in a single experiment. The axes of Fig. 5.3 give the outgoing pion transverse and longitudinal momenta, in the target rest frame. Some labeled straight lines give the pion angle relative to the incoming beam. The three solid elliptical curves each correspond to a fixed value of recoil mass m_X . The outermost (dashed-dotted) curve has $m_X = m_N$ and thus corresponds to the quasielastic process $\gamma N \rightarrow \pi N$, and also marks the kinematic limit of pion momenta. The solid curve has $m_X = 2$ GeV, and the dotted curve has $m_X = 3.5$ GeV. Thus the region between the solid curve and the outermost curve is the resonance region, and the region from the dotted curve to the solid curve is the continuum region. The segment above the grey band is the region where direct pion production dominates. This is the "good region." (As a side note, the grey band is straighter than one might have guessed, especially since it is made up of two parts. The central part comes from the fragmentation process growing larger. Both ends come from VDM, as modeled in an earlier note, which was conservative in estimating the size of the VDM contributions.) Finally comes the important dashed elliptical curve, which has a constant x , specifically $x = 0.7$ in this case. It may be seen that one could thinkably measure the putative scaling function in the resonance region at small pion angles, and then by moving to larger angle, follow its behavior at the same x but larger m_X (and larger $|t|$) well out of the resonance region, before running into a region where fragmentation or soft processes dominate.

(As another aside, lines of constant $|t| \neq 0$ on this plot would be parabolas opening to the right, and passing through the small line segment between the origin and the lower (negative) limit of k_L ; $|t| = 0$ occurs along the positive k_L axis.)

5.4 resonance bumps vs. the scaling curve

There is always a resonance region. In plots of $F(x, s, t)$ vs. x , the bumpy resonance region slides to the right with increasing $|t|$. In the corresponding DIS case the bumps slide neatly down the curve, with the resonance/smooth curve ratio observed to stay the same, for most resonances. Within pQCD, this is expected theoretically [51] as a consequence of the known behaviors of the scaling curve as $x \rightarrow 1$ and the predicted falloff of the resonance transition form factors at high Q^2 . It can be shown that the resonance/continuum constancy is consistent with pQCD in the semi-exclusive case also.

One needs to find the behavior of

$$F_{res}(x, s, t) = \frac{d\sigma}{dx dt}(\gamma N \rightarrow \pi R) / \frac{d\hat{\sigma}}{dt}(\gamma q \rightarrow \pi q') \quad (5.16)$$

at (say) the resonance peak for large $|t|$ (and $x \rightarrow 1$). The denominator in this limit is

$$\frac{d\hat{\sigma}}{dt}(\gamma q \rightarrow \pi q') = g(t/s)|t|^{-3}, \quad (5.17)$$

where $g(t/s)$ is a known function (see Equ. (5.13)) which does not go to zero for t/s finite.

The numerator for a finite width resonance can be approximated by (for $x \rightarrow 1$),

$$\begin{aligned} \left(\frac{d\sigma}{dx dt} \right)_{res} &\approx \frac{|t|}{2m_X} \left(\frac{d\sigma}{dm_X dt} \right)_{res} \\ &\approx \frac{|t|}{2m_R} \left(\frac{d\sigma}{dt} \right)_{res} \frac{\Gamma/2\pi}{(m_X - m_R)^2 + \Gamma^2/4} \end{aligned} \quad (5.18)$$

where Γ is the width of the resonance and I have used a simple lorentzian form to give the resonance shape. The pQCD scaling rules [56] tell us that

$$\left(\frac{d\sigma}{dt} \right)_{res} = \frac{d\sigma}{dt}(\gamma N \rightarrow \pi R) = f(t/s)|t|^{-7} \quad (5.19)$$

where $f(t/s)$ is not known but in general it should not go to zero for finite t/s . Thus,

$$\left(\frac{d\sigma}{dx dt} \right)_{res \text{ peak}} \approx \frac{1}{\pi m_R \Gamma} f(t/s)|t|^{-6}, \quad (5.20)$$

and

$$F_{res\ peak}(x, s, t) \approx \frac{1}{\pi m_R \Gamma} \frac{f(t/s)}{g(t/s)} |t|^{-3}. \quad (5.21)$$

Thus,

$$F_{res\ peak}(x, s, t) \propto (1-x)^3. \quad (5.22)$$

for fixed t/s , using $1/t \propto (1-x)$ for $x \rightarrow 1$.

This is how the height of a resonance peak falls with x as $x \rightarrow 1$. It is also precisely the pQCD expectation for the scaling curve. Hence the resonance/continuum ratio is in general constant for fixed t/s , at least at high $|t|$, similarly to what is seen in DIS.

In DIS, the Delta(1232) is an exception, as it falls markedly with Q^2 [57, 58]; Q^2 in lepton scattering is the analog of $-t$ in hard meson photoproduction. It will be interesting to see if the Delta(1232) disappears with increasing $|t|$ and if the, say, $S_{11}(1535)$ stays up at high $|t|$. Recall that in pQCD, the disappearing Delta in electron scattering is explained as an accident having to do with the specifics of the Delta and nucleon wave functions [59]. One should not expect this to be necessarily replicated in pion photoproduction since the integrals over the distribution amplitudes will involve different weightings.

5.5 Conclusions and Discussion

Semi-exclusive processes give an opportunity to extend the studies of scaling and duality, which in deep inelastic scattering have been fruitful in verifying our understanding of QCD and in pushing our effort to deepen that understanding.

It appears that scaling in the sense that the cross section is directly related to a scaling function that depends, up to logarithmic corrections, on just one variable. The scaling variable for semi-exclusive processes, given in the text, is related to the momentum fraction of the struck quark, just like the scaling variable in deep inelastic scattering. However,

scaling, at least as I have been able to present it in this chapter, works in semi-exclusive process only when the pion is produced directly off the same quark that absorbs the incoming photon. I have been able to show, theoretically, that such a scaling region does exist.

One should bear in mind that there are soft kinematic regions where one does not know where the pion comes from, and fragmentation regions where the pion is produced at some remove from the fundamental process that initiates the reaction. I do not know of a scaling function for these regions, and it is not trivial that one can avoid them, but one can. One should also bear in mind that a certain amount of initial energy is needed to be able to produce a scaling region. For incoming photon lab energy 16 GeV or below and our present estimates of the vector meson dominance contributions, it does not appear that there is a region where VMD is not the biggest process for photoproduction, at least if one does not make any additional cuts. One can consider an "isolation cut," a requirement that there be no other particles collinear with the pion, but this will work best to suppress contributions from the ordinary, semi-exclusive parton fragmentation process. However, another possibility is to have the photon off shell, since then the vector meson propagator is significantly reduced, reducing the VMD contributions without there being an equal reduction for other contributions. I am hopeful that using electroproduction can make the incoming energy requirement low enough to fit an upgraded CEBAF range, but am deferring detailed elaboration.

The existence of a scaling region also allows one to consider the inclusive-exclusive connection with the resonance region. Will the resonance bumps average out to the smooth scaling curve measured at higher $-t$ and evolved to lower $-t$? Will the resonance peak to scaling curve ratio be independent of t ? In deep inelastic physics, it does appear that the final state interactions which produce the resonance are irrelevant to the overall rate of

resonance region production, if one does a suitable average. And I have shown that for the semi-exclusive case, as in the deep inelastic case, the resonance to continuum ratio should be constant, barring special circumstances. A special circumstance in the deep inelastic case occurs for the $\Delta(1232)$, which disappears into the scaling curve with increasing Q^2 . One would like to know if similar phenomena occur in other situations.

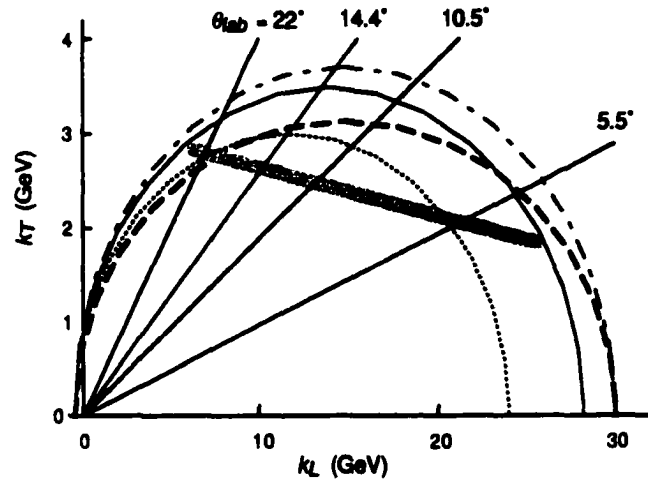


Figure 5.4: Kinematic regions relevant to studying duality in $\gamma N \rightarrow \pi X$ for 30 GeV incoming photons. The upper dashed-dotted line is the overall kinematic limit, and corresponds to $\gamma N \rightarrow \pi N$. The other solid and dotted elliptical lines have m_X of 2 and 3.5 GeV, respectively. Between the solid and dashed-dotted elliptical lines lies the resonance region. Above the grey line soft processes and fragmentation processes are small, and direct pion production dominates. Hence the region between the grey line and the solid elliptical line is the region that can be smoothly compared to the resonance region. The dashed elliptical curve is for x fixed at 0.7.

Appendix A

fragmentation functions

A.1 Carlson-Wakely fragmentation functions

Prior to 1999 the fragmentation functions used were found in the Appendix of a paper by Carlson and Wakely [4]. Briefly, the fragmentation of quarks into pions contains a part D_p if the primary quark is a valence quark in the pion, and also a secondary part D_s for any quark-pion combination. Three examples are

$$\begin{aligned} D_{\pi^+/u} &= D_p + D_s, & D_{\pi^0/u} &= \frac{1}{2}D_p + D_s, \\ D_{\pi^-/u} &= D_s. \end{aligned} \tag{A.1}$$

At the benchmark scale (which taken to be 29 GeV),

$$D_p = \frac{5}{6}(1-z)^2 \quad \text{and} \quad D_s = \frac{5}{6} \frac{(1-z)^4}{z}. \tag{A.2}$$

These forms lead to good fits to the $e^+e^- \rightarrow \pi + X$ data, and so were used. At the time of reference [4], the known fragmentation functions were more than a decade old and no longer fit up-to-date data. Since then a number of other modern fragmentation functions have appeared [27], which also match data. At the point in time when these were used, there

was not any data available to make one fit more desirable than another. The benchmark gluon fragmentation function is

$$D_{\pi/g} = \frac{2(1-z)^3}{3z}. \quad (\text{A.3})$$

A.2 Newer form of Carlson-Wakely

Recent HERMES data suggests that the “unfavored” fragmentation function (e.g., for a u-quark fragmenting to a π^-) is larger than what I had been using [47]. So the best course of action seemed to reparameterize the fragmentation function to fit the newly available data. In the new parameterization the sum determined from $e^+e^- \rightarrow \pi^\pm X$,

$$\frac{1}{\sigma} \frac{d\sigma(\pi^+ + \pi^-)}{dz} = D_p + 4D_s, \quad (\text{A.4})$$

is unchanged but the ratio of unfavored or secondary fragmentation function to primary (or favored minus unfavored) fragmentation function is given by

$$D_s(z)/D_p(z) = 0.5(1-z)^{0.3}/z, \quad (\text{A.5})$$

where z is the fraction of quark momentum that goes into the pion.

Bibliography

- [1] D. Adams *et al.*, Phys. Lett. B **329**, 399 (1994); Phys. Lett. B **336**, 125 (1994); Phys. Lett. B **357**, 248 (1994); P. L. Anthony *et al.*, Phys. Rev. Lett. **71**, 959 (1993); K. Abe *et al.*, Phys. Rev. Lett. **74**, 346 (1995); Phys. Rev. Lett. **75**, 25 (1995); Phys. Lett. B **364**, 61 (1994).
- [2] L. L. Frankfurt *et al.*, Phys. Lett. B **230**, 141 (1989); F. E. Close and R. G. Milner, Phys. Rev. D **44**, 3691 (1991); B. Adeva *et al.*, Phys. Lett. B **369**, 96 (1996).
- [3] A. Apian *et al.*,
CERN-SPSC-98-17.
- [4] C. E. Carlson and A. B. Wakely, Phys. Rev. D **48**, 2000 (1993).
- [5] Similar processes in the context of e^+e^- annihilation were discussed by V. N. Baier and A. G. Grozin, Phys. Lett. **96B**, 181 (1980) and by Th. Hyer, Phys. Rev. D **48**, 147 (1993), *ibid.*, **50**, 4382 (1994).
- [6] I.S. Barker, A. Donnachie, and J.K. Storrow, Nucl. Phys. **B95**, 347 (1975).
- [7] T. Gehrmann and W. J. Stirling, Phys. Rev. D **53**, 6100 (1996).
- [8] M. Glück, E. Reya, M. Stratmann, and W. Vogelsang, report hep-ph/9508347 (DO-TH-9513; RAL-TR-95-042).

- [9] F. Buccella and J. Soffer, *Phys. Rev. D* **48**, 5416 (1993); C. Bourrely and J. Soffer, *Phys. Rev. D* **53**, 4067 (1996).
- [10] J. Huston *et al.*, *Phys. Rev. D* **51**, 6139 (1995).
- [11] H. Olsen and L. C. Maximon, *Phys. Rev.* **110**, 589 (1958).
- [12] F. R. Artunian, I. I. Goldman, and V. A. Tumanian, *Sov. Phys. JETP* **18** 218 (1964); F. R. Artunian and V. A. Tumanian, *Phys. Lett.* **4**, 176 (1963); R. H. Milburn, *Phys. Rev. Lett.* **10**, 75 (1963).
- [13] H.-N. Li and G. Sterman, *Nucl. Phys.* **B381**, 129 (1992).
- [14] E. Braaten, *Phys. Rev. D* **28**, 524 (1983).
- [15] F.-M. Dittes and A. V. Radyushkin, *Sov. J. Nucl. Phys.* **34** 293 (1981) [*Yad. Fiz.* **34**, 529 (1981)]; R. D. Field, R. Gupta, S. Otto, and L. Chang, *Nucl. Phys.* **B186**, 429 (1981); M. H. Sarmadi, U. of Pittsburgh Report, Ph. D. thesis (1982); E. Braaten and S.-M. Tse, *Phys. Rev. D* **35**, 2255 (1987).
- [16] J. J. Peralta, A. P. Contogouris, B. Kamal and F. Lebessis, *Phys. Rev. D* **49**, 3148 (1994).
- [17] A. Afanasev, C. Carlson, and C. Wahlquist, *Phys. Lett. B* **398**, 393 (1997).
- [18] P. Aurenche *et al.*, *Phys. Lett.* **135B**, 164 (1984); E. Auge *et al.*, *Phys. Lett.* **168B**, 163 (1986).
- [19] R. D. Ball, S. Forte, and G. Ridolfi, *Phys. Lett. B* **378**, 255 (1996).
- [20] S. J. Brodsky, M. Burkardt, and I. Schmidt, *Nucl. Phys. B* **441**, 197 (1995).
- [21] S. J. Brodsky and E. L. Berger, *Phys. Rev. D* **24**, 2428 (1981).
- [22] See also J. A. Hassan and D. J. Pilling, *Nucl. Phys. B* **187**, 563 (1981).

- [23] M. Glück, E. Reya, and A. Vogt, *Phys. Rev. D* **46**, 1973 (1992); P. Aurenche, M. Fontannez, and J. P. Guillet, *Z. Phys. C* **64**, 621 (1994); G. A. Schuler and T. Sjöstrand, *Z. Phys. C* **68**, 607 (1995).
- [24] J. Babcock, E. Monsay, and D. Sivers, *Phys. Rev. D* **19**, 1483 (1979).
- [25] See for example the Appendix to S. J. Brodsky, T. Kinoshita, and H. Terazawa, *Phys. Rev. D* **4**, 1532 (1971).
- [26] Review of Particle Properties, R. M. Barnett *et al.*, *Phys. Rev. D* **54**, 1 (1996).
- [27] J. Binneweis, B. A. Kniehl, and G. Kramer, *Z. Phys. C* **65**, 471 (1995) and *Phys. Rev. D* **52**, 4947 (1995); R. Jakob, P. J. Mulders, and J. Rodrigues, report hep-ph/97043
- [28] See for example, Bernd A. Kniehl hep-ph/9709261 or D. de Florian and W. Vogelsang hep-ph/9712273. 35, NIKHEF 97-018, VUTH 97-7.
- [29] M. Glück, E. Reya, and A. Vogt, *Z. Phys. C* **67**, 433 (1995).
- [30] A. P. Contogouris, B. Kamal, Z. Merebashvili, and F. V. Tkachov, *Phys. Rev. D* **45**, 4092 (1993) and *Phys. Lett. B* **304**, 329 (1993).
- [31] D. L. Adams *et al.*, *Phys. Lett. B* **261**, 197 (1991); W. Vogelsang and A. Weber, *Phys. Rev. D* **45**, 4069 (1992).
- [32] P. L. Anthony *et al.*, SLAC-PUB-8049 (1999).
- [33] A. Afanasev, C. Carlson, and C. Wahlquist, *Phys. Lett. B* **398**, 393 (1997).
- [34] A. Afanasev, C. Carlson, and C. Wahlquist, *Phys. Rev. D* **58**, 054007 (1998).
- [35] D. De Florian and W. Vogelsang, *Phys. Rev. D* **57**, 4376 (1998); B. A. Kniehl, Talk at Ringberg Workshop, hep-ph/9709261; M. Stratmann and W. Vogelsang, Talk at Ringberg Workshop, hep-ph/9708243; J. J. Peralta, A. P. Contogouris, B. Kamal and F. Lebessis, *Phys. Rev. D* **49**, 3148 (1994).

- [36] R. J. Apsimon *et al.*, *Z. Phys. C* **43**, 63 (1989).
- [37] I. Abt *et al.*, *Phys. Lett. B* **328**, 176 (1994).
- [38] M Derrick *et al.*, *Z. Phys. C* **67**, 227 (1995).
- [39] G. Schuler and T. Sjöstrand, *Nucl. Phys. B* **407**, 539 (1993); T. Sjöstrand, *J. Phys. G* **22**, 709 (1996). The physics described in these articles has been implemented as part of the PYTHIA event generation code. See T. Sjöstrand, *Comput. Phys. Commun.* **82**, 74 (1994).
- [40] A. Pautz and G. Shaw, *hep-ph/9710235*.
- [41] L. H. O'Neill *et al.*, *Phys. Rev. D* **14**, 2878 (1976).
- [42] P. Bosetti *et al.*, *Nucl. Phys. B* **54**, 141 (1973).
- [43] E. Beier *et al.*, *Phys. Rev. D* **18**, 2235 (1978).
- [44] D. Wisner, Ph. D. thesis, University of Wisconsin, 1977 (unpublished).
- [45] S. I. Manayenkov, report DESY 99-016, *hep-ph/9903405*.
- [46] W. Melnitchouk, J. Speth, and A. W. Thomas, *Phys. Lett. B* **435**, 420 (1998); W. Melnitchouk and J.C. Peng, *Phys. Lett. B* **400**, 220 (1997); W. Melnitchouk and A. W. Thomas, *Phys. Lett. B* **377**, 11 (1996); U. K. Yang and A. Bodek, *hep-ph/9809480*.
- [47] N. Makins, *Proceedings of CEBAF Workshop on Physics and Instrumentation with 6-12 GeV Beams*, ed. S. Dytman, H. Fenker, and P. Roos, JLab, Newport News, June 1998, p.97; Ph. Geiger, *Measurement of Fragmentation Functions at HERMES*, Ph. D. Thesis, Ruprecht-Karls-Universität, Heidelberg, 1998.
- [48] C. Adloff *et al.*, *hep-ex/9810020*.

- [49] E. D. Bloom and F. J. Gilman, *Phys. Rev. Lett.* **25** (1970) 1140; *Phys. Rev. D* **4** (1971) 2901.
- [50] A. DeRújula, H. Georgi, and H. D. Politzer, *Ann. Phys. (N. Y.)* **103**, 315 (1977).
- [51] C. E. Carlson and N. C. Mukhopadhyay, *Phys. Rev. D* **41**, 2343 (1990).
- [52] N. Dombey and R. T. Shann, *Phys. Lett. B* **42**, 486 (1972); G. B. West, *Phys. Lett. B* **46**, 486 (1973); A. Calogeracos, N. Dombey, and G. B. West, hep-ph/9406269.
- [53] S. J. Brodsky, M. Diehl, P. Hoyer, S. Peigne, *Phys. Lett. B* **449**, 306 (1999).
- [54] A. Afanasev, C. E. Carlson, and C. Wahlquist, *Phys. Rev. D* **61**, 054007 (2000).
- [55] J. F. Owens, *Rev. Mod. Phys.* **59**, 465 (1987).
- [56] S. J. Brodsky and G. Farrar, *Phys. Rev. Lett.* **31**, 1153 (1973), *Phys. Rev. D* **11**, 1309 (1975); V. A. Matveev, R. M. Muradyan, and A. N. Tavkhelidze, *Lett. Nuovo Cimento* **7**, 719 (1973).
- [57] P. Stoler, *Phys. Rev. Lett.* **66** 1003 (1991); *Phys. Rev. D* **44** 73 (1991); *Phys. Rep.* **226**, 103 (1993); G. Sterman and P. Stoler, *Ann. Rev. Nucl. and Part. Sci.* (in press).
- [58] C.E. Carlson and N.C.Mukhopadhyay, *Phys. Rev. D* **47** (1993) R1737.
- [59] C.E. Carlson and J.L. Poor, *Phys. Rev. D* **38**, 2758 (1988); G.R.Farrar, H. Zhang, A.A. Oglublin, and I.R. Zhitnitsky, *Nucl. Phys. B* **311**, 585 (1989); J. Bonekamp, Bonn report(1989).

Vita

Christian Jens Wahlquist

Born in Ogden, Utah, December 2, 1969. Graduated from Weber State University in 1994 with a Bachelor of Science degree in Physics and a Minor in Mathematics.

Obtained a Master of Science degree in Physics from the College of William and Mary in Virginia in 1996. This dissertation was presented in August 2000 in partial fulfillment of the requirements for the Doctor of Philosophy degree in Physics.